Accepted Manuscript

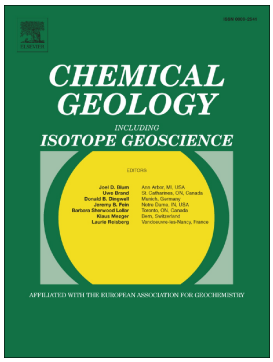

Isotopic characterization of late Neogene travertine deposits at Barrancas Blancas in the eastern Atacama Desert, Chile

J. Quade, E.T. Rasbury, K.W. Huntington, A.M. Hudson, H. Vonhof, K. Anchukaitis, J. Betancourt, C. Latorre, M. Pepper

PII: S0009-2541(17)30270-X
DOI: doi: 10.1016/j.chemgeo.2017.05.004
Reference: CHEMGE 18333

To appear in: *Chemical Geology*

Received date: 13 December 2016
Revised date: 19 April 2017
Accepted date: 1 May 2017

Please cite this article as: J. Quade, E.T. Rasbury, K.W. Huntington, A.M. Hudson, H. Vonhof, K. Anchukaitis, J. Betancourt, C. Latorre, M. Pepper , Isotopic characterization of late Neogene travertine deposits at Barrancas Blancas in the eastern Atacama Desert, Chile, *Chemical Geology* (2017), doi: 10.1016/j.chemgeo.2017.05.004

Isotopic Characterization of late Neogene travertine deposits at Barrancas Blancas in the eastern Atacama Desert, Chile

Quade, J.,[1*], Rasbury, E.T.[2], Huntington, K.W[3], Hudson, A.M.[4], Vonhof, H.[5], Anchukaitis, K.[6], Betancourt, J.[7], Latorre, C.[8], Pepper, M.[1]

[1]*Department of Geosciences, University of Arizona, Tucson, Arizona 85721, USA*

[2]*Department of Geosciences, University of New York at Stony Brook, New York 11797-2100*

[3] *Department of Earth and Space Sciences, University of Washington, Seattle, WA 98195.*

[4] *U.S. Geological Survey, Geosciences and Environmental Change Science Center, P.O. Box 25046, Denver Federal Center, MS 980, Lakewood, CO 80225*

[5]*Max Planck Institute of Chemistry, Hahn-Meitnerweg 155128 Mainz, Germany*

[6]*School of Geography and Development, University of Arizona, Tucson, Arizona 85721, USA*

[7] *U.S. Geological Survey, National Research Program, Water Mission Area, Mail Stop 430, Reston, VA 20192*

[8]*Department of Ecology, Pontificia Universidad Católica de Chile, Alameda 340, Santiago, Chile and Institute of Ecology & Biodiversity (CASEB)*

*corresponding author: quadej@email.arizona.edu
phone: (520)-818-8006
FAX: (520)-621-2672

Keywords: Andes, Atacama Desert, travertine, stable isotopes, U-Pb dating, fluid inclusions, Devils Hole

ABSTRACT

Here we explore the potential of spring-related, surface and subsurface carbonates as an archive of paleoenvironmental change at Barrancas Blancas, located in the broadest and driest sector of the Atacama Desert at 24.5°S. From these deposits we present a new stable isotopic record of paleoenvironmental conditions over portions of the past ~11.5 Ma. U-Pb dates from the carbonates, both surface and subsurface, demonstrate that springs have discharged at this location over much of the last 11.5 Ma, attesting to the exceptional geomorphic stability of the central Atacama. Many of the sampled vein

systems line vertical fissures, and formed within the aquifer before groundwater discharged at the surface. Carbonates in such circumstances should not undergo off-gassing and kinetic fractionation prior to formation, simplifying the interpretation of their isotopic composition. Oxygen isotopic compositions of carbonates are generally high (>-1‰VPDB), and using paleospring water temperatures of 3-13°C reconstructed from clumped isotopes, point to strongly (up to 50%) evaporated water isotope values, like those associated with the hyperarid core of the Atacama Desert today. Carbon isotopic compositions are also high (≥ +3‰ PDB), reflecting a recharge area essentially devoid of plants and dominated by volcanic CO_2, as is the case today. Our isotopic results are very similar to those from the Calama Basin to the north, suggesting that the western face of the Andes between 21-25°S has been highly evaporative and nearly plantless when these springs discharged over the last 11.5 Ma. The spring carbonates at Barrancas Blancas strongly resemble those found at Devils Hole and Furnace Creek in Death Valley, USA, and as such warrant further exploration as potential archives of climate change.

1. Introduction

Spring deposits are receiving increasing recognition as significant archives of paleoenvironmental change in the Atacama Desert (Betancourt et al., 2000; Rech et al. 2002; Quade et al., 2008) and elsewhere (Winograd et al, 1992; Pigati et al., 2014). Springs are fed by meteoric water that falls on the local catchment area, and clastic and mineral deposits associated with springs fed by this rainfall record changing environmental conditions averaged across that recharge area. The stable isotope ratios of

oxygen from mineralized spring deposits are useful in reconstructing changes in rainfall sources and air temperature, whereas those of carbon reflect on the nature and extent of plant cover. Other rare combinations of the isotopes of oxygen and carbon ("clumped isotopes") in carbonates can be used to reconstruct paleotemperatures at the point of mineralization.

Travertine is probably the most common of spring-related mineral deposits, and it forms by the precipitation of carbonate minerals in cold and thermal springs and streams in a wide range of climatic settings (Dictionary of Geological Terms, 1962). Many studies have examined the isotopic systematics of actively forming travertines, often with a view of exploiting their potential as paleoclimate archives (e.g. Usdowski et al., 1979; Amundson et al., 1987; Matsuoka et al., 2001). Nearly all this work has focused on the surficial travertines, that is, travertine that formed at the surface or downstream of the point of spring discharge. After reaching the surface, spring water can evaporate and off-gas CO_2, sometimes leading to kinetic enrichment of ^{13}C, ^{18}O, and ^{2}H in residual water. This results in well-documented increases in the $\delta^{13}C$ and in some cases the $\delta^{18}O$ values of carbonate that precipitate downstream of the discharge point (Usdowski et al., 1979; Matsuoka et al., 2001). The rates of non-equilibrium loss of isotopes species are controlled a number of factors, such as water temperature, humidity, pCO_2 in the water and air, distance from the discharge point, water turbulence, and so forth. These factors are largely unknowable in the past, compromising the use of oxygen and carbon isotopes in surface travertines for paleoclimate reconstruction.

Far less recognized in the published record are carbonates that form in the subsurface, cementing the conduits that feed spring discharge at the surface. Here the circumstances

of carbonate formation are quite different. By definition the conduits lie in the saturated zone, and as such do not experience the kind of rapid losses into the gas phase (i.e. evaporation and CO_2 off-gassing) experienced by spring water at the surface. These types of subsurface travertines or vein carbonates are recognized globally (e.g. Avigour et al., 1990; Uysal et al., 2007; De Filippis et al., 2012) but are perhaps best characterized in several localities in Death Valley USA, namely at Devils Hole and Furnace Creek (Winograd et al., 1985, 1992). There, carbonates cement the walls of the conduits in the aquifer systems that fed and still feed the springs in this area. They have accreted evenly and slowly (0.7mm/1000 yrs) through glacial and interglacial cycles during the last several million years. The slow rates of accretion in a saturated underwater environment ensure equilibrium conditions of formation, to the extent that the subsurface vein carbonates at Devils Hole have been used by some studies to test and define equilibrium fractionation factors for the oxygen and carbon isotope systems (Coplen et al., 1994; Coplen, 2007; Kluge et al., 2014). This has permitted the reconstruction of changes in vegetation cover and recharge conditions in the high elevation catchment of the Devil's Hole system. These features of subsurface carbonates make them excellent potential paleoclimate archives (Winograd et al., 1985, 1992).

In this paper we present results from travertines at Barrancas Blancas that formed at the western foot of the Andes in the Atacama Desert of Chile (Fig. 1). This sector of the Atacama Desert between 18-26°S is arguably the driest region of the world, in its hyperarid core receiving <10mm/yr of precipitation below 1500 masl. The causes of this aridity are well known and include a mid-latitude position (18-30°S) south of subtropical Hadley circulation; orographic blockage of dominantly easterly moisture sources by the

high-standing Andes (Houston and Hartley, 2003); continentality; decreased evaporation from the nearby Pacific Ocean by cold coastal currents (Hartley et al., 2005); and thermal inversion over the Pacific Ocean, thus inhibiting convection, and confining moisture to <1000 m (Garreaud et al., 2010). Most of these features have probably characterized this latitude of South America since at least the early Cenozoic (Marty et al., 1988; Randall, 1998; Hartley et al., 2005; Canavan et al., 2014). However, interpretation of various proxies has led to a range of estimates from Oligocene to Quaternary for the onset of hyperaridity that characterizes the climate of the Atacama today (Sillitoe and McKee, 1996; Hartley and Chong, 2002; Dunai et al., 2005; Rech et al. 2006; Amundson et al., 2012; Sáez et al., 2012). Moreover, some research suggests that hyperarid conditions in the mid-Miocene gave way to wetter conditions in the Pliocene (Sáez et al., 2012; de Wet et al., 2015; Evenstar et al., 2015) in possible response to strengthening of El Niño-like conditions at that time (i.e. warmer coastal waters decrease the thermal inversion, which in turn favors advection of moisture inland – see Garreaud et al., 2010). Isotopic records from subsurface and surface carbonates such as at Barrancas Blancas can potentially address the many questions surrounding the temporal and spatial variability of hyperaridity in the Atacama, provided that the carbonates are datable and their isotopic systematics are well understood. Our ultimate goal is to reconstruct long-term hydroclimate in the recharge area (the neighboring high western Andes and Puna Plateau) of the Barrancas Blancas paleosprings. Here we present our initial survey, dating, and stable ($\delta^{13}C$, $\delta^{18}O$, Δ_{47}) isotopic characterization of all types of travertine from several key locations, but with particular emphasis on the cements from the subsurface vein systems.

2. Description of the Springs and Spring Deposits

Barrancas Blancas is situated in the southeast quadrant of the Salar de Punta Negra basin, ~200 km southeast of the coastal city of Antofagasta (Fig. 1). The Cordillera Domeyko borders the western side of the valley, and the loftier western Cordillera of the Andes on the east side. Volcán Llullaillaco (6739 m), 35 km northeast of Barrancas Blancas and one of the world's highest volcanoes, has one of the highest snowlines in the world at ~6500 m, further testimony to the hyperaridity of the region. Large alluvial fans descend steeply down the west flank of the Andes south of Llullaillaco, and onto the margins of Salar de Punta Negra (Fig. 1), a large phreatic playa in the valley bottom. Barrancas Blancas is situated on the distal reach of one of these fans. Barrancas Blancas roughly translates as "white bluffs", because of the white travertine that caps the low hills and cliffs in this area. To our knowledge, the basic geology and hydrology of these deposits has not been previously described except at a brief reconnaissance level (Vila and Chong, 1972) so we describe them here before presenting our isotopic results.

There are at least four very small but active cold-water (5-10°C) springs at Barrancas Blancas (Fig. 2). Only the largest spring, associated with sample SPN-25 in area C, has sufficient flow to support a small creek that flows down slope a few hundred meters before disappearing below the ground surface. These springs are fed by moisture derived mostly from the higher Andes at >4000m, which receive much more rain and snow (≥100 cm/yr) than local elevations (≤30-50 mm/yr) around the springs at ~ 3000 m. The geomorphic position of the springs near the toe of a west-dipping fan also points to

recharge from the nearby Andes to the east. All four of the springs and seeps are on or just upslope of visible fault traces, suggesting that the faults intercept the water table at depth, bringing it to the surface (Fig. 2). The faults are part of the Barrancas Blancas normal fault system (Mpodozis et al., 1993) that cuts the toes of alluvial fans along the east side of the Salar de Punta Negra basin. Springs and spring discharge deposits of various types can be found in many similar locations along the base of the Andes to the north (Betancourt et al., 2000; Rech et al., 2002; Quade et al., 2008). Fault localization of modern spring discharge is a common feature in the Atacama Desert and in the other arid and tectonically active deserts such as the Mojave Desert of the western U.S.A. (e.g. Pigati et al., 2014).

The travertines at Barrancas Blancas are conspicuous and extensive, and nearly continuously cover a ~5km^2 area. Modern gullies cut through all the major travertine-covered areas, exposing up to 12 m of the sedimentary deposits, which in some cases rest directly on an undated ignimbrite. The deposits are a mixture of interlayered travertine and alluvial-fan sediments (Fig. 3b-c). The fan sediments are dominated by very coarse sand and imbricated, fine to coarse gravels dipping gently (1-3°) westward. Alluvial clasts are dominated by ignimbrite and granite, with a minor component of reworked travertine fragments.

We described and sampled the travertines at a reconnaissance level in four main areas (A-D from north to south) shown on Figure 2. Radiometric dating was essential for establishing the relative stratigraphic order of these deposits, due the lack of cross-cutting relationships and exposure between and sometimes within areas. Two stratigraphic profiles were described in detail at two locations (Figs. 2, 4: AD10-117 in area A, and

AD10-121 in area D) where gullies expose 7 to 11 meters of interlayered travertine and alluvial fan sediments. The horizontally bedded travertines in these areas consist of stacked or isolated layers of micrite to dense, yellow, radiating masses of sparry carbonate (Fig. 3). Erosional unconformities interrupt sedimentation at several levels in both profiles, denoted by rip-ups of travertine in sand resting on scoured surfaces of travertine (Fig. 4a: AD10-117, levels +2.6 and +5.4m; Fig. 4b: AD10-121, levels +1.0, +3.9, and +7.2 m).

What is truly unique and significant about the Barrancas Blancas deposits, and a key focus of our sampling, are the abundant vertical fissures filled with travertine (Fig. 3 d,e). Like horizontal travertine, the veins are mostly composed of sparry white, yellow, and in a few cases bright orange (Fig. 3a) carbonate. Vein widths vary from a few to ~50 cm. Other aspects of the vein fill are quite variable: many contain breccia fragments of older spar or gravel clasts, a few are stained dark gray with MnO_2, and many are symmetrically cemented on both sides of individual fractures. The latter feature suggests cementation on both walls of the fissure as it gradually opened, probably in response to ongoing tectonic extension. In some outcrops at Barrancas Blancas, the vertical veins can be seen to transition into thick horizontal ones, providing the opportunity to evaluate the impact of kinetic effects on the $\delta^{13}C$ and $\delta^{18}O$ values after spring water reaches the surface.

3. Laboratory Methods

3.1 U-Pb Dating

Hand specimens were cut and polished and subjected to phosphor imaging to map the

distribution of uranium. Radioactivity from the presence of U causes Eu^{2+} in the imaging plate to oxidize to Eu^{3+}. Upon scanning (or exposure to light), Eu^{3+} reverts to Eu^{2+} and emits light in proportion to local U content, which is then detected in the scan (Cole et al., 2003). Areas with high U/Pb were sampled to improve the likelihood of obtaining higher precision ages. Samples were crushed to medium to coarse sand-sized pieces and further selected to avoid discoloration and inclusions. The selected crushed fragments were sonicated in distilled water three times to remove any dust or unwanted material. After drying in the clean lab, the samples were weighed and spiked with a mixed ^{205}Pb-^{236}U tracer. The samples were dissolved in dilute nitric acid until the effervescence stopped and then capped and placed on the hotplate for at least 12 hours. Sample AD10-111 alone was left on a hotplate for 72 hours, to test if more heating time might be needed for spike equilibration. After heating, the samples were dried down and then redissolved in 0.7 N HBr and eluted in equilibrated Biorad AG1 X8 100-200 mesh-anion exchange resin to separate U and Pb from other elements. Eluent was collected and dried down, then redissolved in nitric acid for elution on the same columns to isolate U from Ca and other ions. The eluent containing U was then dried, loaded on Re filaments with graphite, and run as a metal on a Finnigan MAT 262 TIMS at between 1800-1900^{o}C. For AD10-111, U was run on a Nu Multi-collector ICPMS and bracketed with natural U to correct for fractionation and drift. The Pb aliquots were loaded on Re filaments with a silica gel (Gerstenberger and Hasse, 1997) and run between 1300-1400^{o}C on a Finnigan MAT 262, except for AD10-111, which was run on a IsotopX Phoenix62 TIMS. Both instruments are located at the University of New York at Stony Brook. Data reduction was done with PbDAT followed by IsoExcel (Ludwig, 1993, 2003). All U-Pb dating errors on ages

are reported as percent uncertainty at 2σ.

3.2 Isotopic Analysis of Carbonate

Samples were slabbed and micro-drilled for ~0.5 to 1 mg of powder. As with our sampling for U-Pb, areas of discoloration and secondary cementation (which were uncommon) were avoided. Carbonate analyzed for $\delta^{18}O$ and $\delta^{13}C$ values was first heated at 250°C for 3 hours *in vacuo* to remove volatile contaminants. Laboratory tests show that carbon and oxygen isotope ratios of inorganic carbonates remain unchanged after roasting at 250°C (Wierzbowski, 2007). In organic-rich samples, variance in isotopic measurement is reduced when volatiles associated with organic matter are removed by roasting. Stable isotopic analyses used an automated sample preparation device (Kiel III) attached directly to a Finnigan MAT 252 mass spectrometer at the University of Arizona. Measured $\delta^{18}O$ and $\delta^{13}C$ values were corrected using internal laboratory standards calibrated to NBS-19. Precision of repeated standards is ±0.11‰ for $\delta^{18}O$ (1σ). Carbonate isotopic results are reported using standard δ-per mil notation relative to VPDB. Values of water $\delta^{18}O_w$ in equilibrium with the carbonates were calculated using the calcite-water thermometry equation of Kim and O'Neil (1997).

3.3 Isotopic Analysis of Spring and Well Water

Springs were sampled at the discharge point to ensure against any evaporation or off-gassing by spring water after discharge. At each sample site, 15mL centrifuge tube was

completely filled (to remove any head space) with unfiltered water, then sealed with Teflon and electrician's tape, kept in the dark during transport, and refrigerated in the laboratory. $\delta^{18}O$ (SMOW) of water samples were measured using the CO_2 equilibration method on an automated sample preparation device attached directly to a Finnigan Delta S mass spectrometer at the University of Arizona. The δD values of water were measured using an automated chromium reduction device (H-Device) attached to the same mass spectrometer. The values were corrected based on internal laboratory standards, which are calibrated to SMOW and SLAP. The analytical precision for $\delta^{18}O$ and δD measurements is 0.08‰ and 0.6‰, respectively (1σ). Water isotopic results are reported using standard δ-per mil notation relative to VSMOW.

3.4 Isotopic Analysis of Fluid Inclusions

Roughly 0.72 to 1g of carbonate cut into prisms were extracted for δD and $\delta^{18}O$ analysis of fluid inclusions of four samples. At least two replicates of each sample were run. The prisms were crushed with a percussion device and the released water analyzed for δD and $\delta^{18}O$ using a Thermo-Finnigan TC-EA pyrolysis furnace at Vrije Universiteit, Amsterdam (see Vonhof et al., 2006, 2007, for details of the methods used). Isotopic values of inclusion waters, henceforth referred to as $\delta^{18}O_{inclusw}$ and $\delta D_{inclusw}$, are reported as per mil (‰) deviations compared to VSMOW. Analytical precision at 1σ of reference waters injected into the crusher is 1.4‰ for δD and 0.3‰ for $\delta^{18}O$.

3.5 Clumped isotope analysis

Clumped isotope analysis ($\delta^{18}O$, $\delta^{13}C$ and Δ_{47}) of carbonate samples was performed at the University of Washington. Carbonate samples and standards (2-5 mg) were digested for 10 minutes at 90 °C in a common bath of phosphoric acid (specific gravity 1.90-1.95). The evolved CO_2 was cryogenically separated from water and purified on an automated stainless steel vacuum line, which used He as the carrier gas to pass the CO_2 through a Porapak Q trap (50/80 mesh, 15 cm long, 4.5 mm ID, 0.635 mm OD) held between -10°C and -20°C for a transfer time of 15 minutes. For each of four carbonate sample unknowns, a carbonate standard was digested and purified using the same procedure. Purified CO_2 was transferred to pyrex break seals and loaded into an automated 10-port tube cracker inlet system on a Thermo MAT 253 mass spectrometer configured to measure masses 44-49 inclusive. All Δ_{47} values include an automatically measured pressure baseline background measurement (or PBL; see He et al., 2012). Δ_{47} values were calculated using the methods of Huntington et al. (2009), with the exception that data were calculated using the ^{17}O correction parameters of Brand et al. (2010), as recommended by Schauer et al. (2016) and Daëron et al. (2016). Δ_{47} values were corrected to the absolute reference frame (ARF) of Dennis et al. (2011) using analyses of CO_2 heated to 1000°C or equilibrated with water at 4 and 60 °C. Data reduction scripts are provided by Schauer et al. (2016). Carbonate standards for these analyses include internal standards calibrated to NBS-19 as well as C64 and COR, and ETH international standards, which are all reported relative to VPDB ($\delta^{13}C$, $\delta^{18}O$) and ARF (Δ_{47}); complete clumped isotope data are provided in the online Data Repository Table A.1. Sample Δ_{48} values were used to screen for contamination (Δ_{48} > 2 ‰ rejected). All samples were

analyzed in replicate (3–4 runs) to minimize standard analytical error. Carbonate temperature ($T(\Delta_{47})$) was calculated from measured Δ_{47} values using a slightly modified version of Equation 1 of Kelson et al. (2017, no acid fractionation; see Table 4 footnote), which was produced using the same analytical methods and calculation methods used on our samples and which experiments show is appropriate for a wide range of natural carbonates. Preliminary comparisons indicate that this calibration is consistent with other calibration studies (Daëron et al., 2016; Sierra Petersen, personal communication, 2017; Cedric John, personal communication, 2017), including other inorganic carbonate calibrations (Kluge et al. 2015) and travertine/tufa-specific calibrations (Kele et al. 2015).

5. Results

We obtained over 170 stable isotope values from sixteen different sparry carbonate samples. As time and funding permitted, we obtained U-Pb, fluid inclusion, and clumped results on a subset of this larger sampling. We also analyzed nine local spring and well waters.

5.1 Mineralogy and Physical Condition of the Carbonates

Petrographic investigation of Barrancas Blancas carbonates revealed a mix of white to bright orange, sparry, dense, highly crystalline carbonates. Mineralogically, XRD analysis of six separate vein systems (SPN-25, AD10-111, SPN-15A, SPN-18A, SPN-12BX, SPN-12AX) indicated virtually pure calcite, with traces of quartz and but no aragonite. A few layers in samples are siliceous sinter, which appears to be primary

because the silica follows evenly along bedding planes, alternating with carbonate. The carbonates are composed of translucent to semi-translucent crystals up to several centimeters in length. The crystals are generally perpendicular to but in some cases radiating off of bedding planes. The carbonates are dense with little porosity or secondary detritus (mostly <1-2%). Carbonate evenly and continuously coats both sides of vertical fractures over several meters. Horizontal carbonate also tends to be evenly layered but is often cut by local erosion and reworking (Figs. 3c, 4). Unlike some spring travertines, there are no clear biologic structures such as leaf impressions, tubes molds, nor algal structures like charophytes. We also found no shells or ostracodes valves.

The sparry carbonates at Barrancas Blancas are readily distinguishable from secondary pedogenic and deeper vadose zone carbonates formed from downward flow (*per descensum*) along fractures. As a class these *per descensum* carbonates are dirty, micritic, and less layered than the spring and groundwater carbonates (Vaniman et al., 1988; Hill et al., 1993). Some of this kind of secondary carbonate does cement bedding planes and shallow fractures at Barrancas Blancas, but was easily avoided in sampling. Because of the low porosity, there is virtually no visible secondary carbonate within the sparry layers of the travertines. The excellent preservation and lack of secondary diagenesis or cementation of the sparry travertines at Barrancas Blancas is probably due to the extremely dry and cold climate in the discharge area.

5. 2 U-Pb dating

Travertine samples returned U concentrations that range from 2.55 to 58.62 ppm and Pb concentrations that range from 0.03 to 0.17 ppm (Table 1). The large range of concentrations is not related to mineralogy, because all the carbonates are calcite.

Differing fluid fluxes between individual vein systems may play a role, with higher fluxes increasing U content. Whatever the cause, high U and low Pb content of the travertines made them excellent targets for dating. The U/Pb ratios range from 15 to 405, and common Pb is low enough that individual data points give the same ages as the isochrons. Because of slightly higher precision we report our dating results using intercept ages that fall on concordia on Tera-Wasserburg plots, which range from 2.079±0.044 (2σ) (Table 1 and Fig. 5, SPN-25) to 11.52±0.43 (2σ) Ma (Table 1 and Fig. 5, AD10-111). We regard all our results as generally reliable, despite the high MSWD returned by two samples, SPN-15 and -16, which clearly show geological scatter. The high MSWD's may be caused by sample inhomogeneity, radiation damage, or secondary cementation by younger carbonate, although we regard the last as least likely, given the dense and pristine appearance of the samples.

The distribution of ages roughly follows sample elevation. The oldest sample (age = 11.52±0.43 Ma), AD10-111, was obtained at the highest elevation (3331m) and well above the modern springs in Area B (Fig. 2). The youngest (age = 2.08±0.04 Ma), SPN-25, comes from lowest elevation (Fig. 2, Area C, 3280m), and within <4 m of the elevation of modern spring discharge. SPN-12, 15, and 16 come from intermediate elevation (~3287-3290m) areas, and they yielded intermediate ages (5.11±0.032 to 10.37±0.68 Ma).

5.3 Stable Isotope Results

$\delta^{13}C$ (PDB) values of all travertines (henceforth $\delta^{13}C_{trav}$ (PDB)) range from +0.9 to

+9.4‰, and $\delta^{18}O_{trav}$ (PDB) values from -5.0 to +5.8 (Table 2), and do not correlate among horizontally ($\delta^{13}C_{trav}$ versus $\delta^{18}O_{trav}$: $r^2 = 0.013$) nor vertically ($r^2 = 0.018$) deposited travertine. Mean $\delta^{13}C_{trav}$ (+5.8±1.2‰) and $\delta^{18}O_{trav}$ (-1.9±1.1) values in vertical fissures are higher than those of horizontal travertine (+5.1±1.7‰; -0.9±1.5), but by <1‰ and <1σ. Horizontal travertine with rip-up surfaces returned values ($\delta^{13}C_{trav}$ =+5.20±1.06‰; -$\delta^{18}O_{trav}$ =1.02±1.12‰) indistinguishable (t-test <80%) from those of other, unscoured horizontal travertine (Table 2).

Detailed analysis from single horizons of horizontal travertine shows that $\delta^{13}C_{trav}$ values tend to be slightly more variable than those of $\delta^{18}O$ values (Fig. 4), but in neither case does within layer variation exceed 2‰. Rip-up clasts of travertine (Fig. 4a: AD10-117b) show the widest range in isotopic variation, suggesting reworking from a variety of older layers.

Isotopic values from local Atacama springs and wells (henceforth $\delta^{18}O_{spring}$, δD_{spring}) in the area are quite high: δD_{spring} (VSMOW) from -39 to -54.4‰, and $\delta^{18}O_{spring}$ (SMOW) from -1.9 to -6.2‰ (Table 3). When cross-plotted in $\delta D/\delta^{18}O$ space (Fig. 6), the Atacama ground and spring waters (Fig. 6: "24.5° this study") fall along a straight line ($r^2 = 0.76$) with a lower slope than that of rainwater from the Atacama (Fig. 6: "LMWL"compiled in Aravena et al., 1999) or globally (Fig. 6: GMWL).

Four fluid inclusion water samples extracted from four travertine samples also yielded high $\delta D_{inclusw}$ (-58±6‰) and $\delta^{18}O_{inclusw}$ (-2.3±1.7‰) values (Table 3). They plot along the same general trend as local spring and well waters sampled at 24.5°S in this study (Fig. 6), and well to the right in $\delta D/\delta^{18}O$ space of the trend defined by local (LMWL) and global (GMWL) rainwater.

5.4 Clumped isotopes

The average Δ_{47} (ARF) value of three to four replicates of each of five samples range from 0.640 ± 0.014 to 0.679 ± 0.016 (Table 4). These Δ_{47} values correspond to temperature estimates ($T(\Delta_{47})$) ranging from 3 ± 4 to 13 ± 4 °C (1SE, Table 4), using a slightly modified version ($\Delta_{47} = (41700/(T°C + 273.15)^2 + 0.13)$ of Equation 1 from Kelson et al. (2017). There is no discernible pattern with age or horizontal versus vertical veins, although the sample size is small (n = 5). Two results from different parts of the same vein (Table 3: SPN12 AZ and AY) returned identical temperatures, suggesting that single vein systems may have formed in thermally stable and uniform conditions. The reconstructed temperatures overlap the range of observed temperatures (5-10°C) of active springs at Barrancas Blancas today.

6. Discussion

6.1 Oxygen isotopic results

Our isotopic results from waters in springs and wells in the Barrancas Blancas area are rather unusual in that they must have experienced significant evaporation as surface water prior to infiltration. In $\delta D/\delta^{18}O$ space, modern water values (Fig. 6: "24.5°S this study") fall along a well-defined ($r^2 = 0.76$) trend with a positive slope of ~3, typical of waters enriched in ^{18}O and ^{2}H by evaporation (Clark and Fritz, 1997) (Fig. 6). The Barrancas Blancas springs in particular are positively offset from presumed source

rainwater and snow ($\delta^{18}O$ ~-10‰ SMOW (Fig. 6)) by up to 8‰ for $\delta^{18}O$. Using simple Rayleigh distillation, this requires as much as 50% loss by evaporation to parent rainfall as it was converted to groundwater. Varying degrees of evaporation are characteristic of groundwater and surface streams from the hyperarid deserts of the world (Clark and Fritz, 1997) such as the Atacama, areas of the nearby western Andes (Fiorella et al., 2015), the eastern Sahara (e.g, Sultan et al, 2000), and Antarctic Dry Valleys (Gooseff et al., 2006).

Godfrey et al. (2003), studying surface water and groundwater in the nearby Andes, concluded that enrichment in ^{2}H and ^{18}O in local groundwater must occur prior to recharge. There are two likely causes for this, both related to the hyperaridity of the Atacama Desert and western Andes. One is evaporation of soil water prior to groundwater recharge. Supporting evidence for significant soil evaporation is that $\delta^{18}O$ values of soil carbonates are the highest in the world in this region, reflecting substantial dewatering of soils by evaporation at all elevations (Quade et al., 2007), snow covered or not. The other cause is sublimation, which strongly enriches surface layers of snow in ^{2}H and ^{18}O in the western Andes (Peña, 1989; Stichler et al., 2001), removing a large proportion of the snow where relative humidity is low. Support for the contribution of sublimated snow to recharge is visible in the similarity of the elevated $\delta^{18}O$ and δD values of local melt water run-off (Alpers and Whitmore, 1990) to that of the Barrancas Blancas springs and local groundwater (Fig. 6: "24.5°S this study").

Published isotopic data on groundwater (listed in Fig. 6 legend and caption) from the Atacama Desert, combined with our new data, display considerable scatter as well as systematic offset to the right of the global and local meteoric lines (Fig. 6). Both these features are consistent with variable evaporation of groundwater starting from a range of

initial rain and snow compositions. Initial $\delta^{18}O$ values appear to range from as low as -12‰ in northern Chile 18-20°S (Magaritz et al., 1989; Fiorella et al., 2015) to -8 to -10‰ (Ortiz et al., 2014; Dettinger and Quade, 2015) in the more southerly sector of the Andes studied here. Groundwater from the area around Barrancas Blancas shows greater enrichment in ^{18}O and ^{2}H by evaporation away from these starting compositions than does groundwater further north, consistent with increasing aridity southwards. The scatter and degree of evaporation seem to increase most sharply south of about 24°S, the latitude of the Rissman et al. (2015) study, and just south of the approximate southern limit of habitability in the western Andes by Native Americans at ~23.5°S.

Turning to the carbonate record, what do the $\delta^{18}O_{trav}$ and $\delta^{18}O_{inclusw}$ values tell about conditions of formation and the history of hyperaridity in the region? Several lines of evidence point to highly evaporated parent water over much of the past 11.5 Ma, similar to the present isotopic composition of spring water and groundwater. Travertine from vertical fissures presents the simplest case, because the water from which it formed should reflect that of recharge water unmodified by later evaporation during discharge over horizontal travertine surfaces. First, $\delta^{18}O_{inclusw}$ (VSMOW) values from the four vertical travertine samples all closely resemble that of modern spring water and groundwater (Fig. 6). $\delta^{18}O_{inclusw}$ (VSMOW) values average -3.1±2.5‰ (Table 2), compared to -4.3±1.6‰ for local spring and well water (Table 2). Although it is possible that oxygen in inclusion water exchanged oxygen in adjacent carbonate, hydrogen in water should not have undergone exchange. Consistent with this, $\delta D_{inclusw}$ (VSMOW) values average -48±10‰, identical to that for average local spring and well water of -48±6 today.

Second, we can use the estimated temperatures of formation $T(\Delta_{47})$ from clumped isotope analysis of 3 to 13°C, combined the average $\delta^{18}O_{trav}$ (PDB) values on the same gas from co-existing horizontal carbonate, to reconstruct past $\delta^{18}O_{spring}$ values. This yields estimated $\delta^{18}O_{spring}$values of about -1.4 to -4‰ (Table 4 (data table and footnotes for methodology); Fig.6, shaded vertical box). The oldest of the dated vertical travertines is 5.1 Ma (Table 1, SPN-12), and so our results indicate that highly evaporated groundwater has been feeding this location at Barrancas Blancas since at least 5.1 Ma. It also shows that in the past, spring water prior to discharge was not hydrothermal but quite cold, as it is in the study area today.

The isotopic difference between vertical and horizontal calcite is small (≤1‰), as is variability in $\delta^{18}O_{trav}$ (± 1.12 for vertical, ±1.48 for horizontal) and $\delta^{13}C_{trav}$ values (±1.24 for vertical, ±1.66 for horizontal). This indicates that horizontal travertine underwent minor evaporation and loss of CO_2 on the surface. The bulk of $\delta^{18}O_{trav}$ and $\delta^{13}C_{trav}$ values all fall in the same ~6‰ range for both vertical and horizontal travertine. This similar range and variability argues against major modification of isotopic values once fluids discharged at the surface. Several other observations support the view that typical spring water at Barrancas Blancas was not significantly modified before precipitating carbonate. One is that filling of vertical veins with carbonate shows that spring water was already saturated with respect to carbonate in the subsurface, and off-gassing and evaporation was not required to induce carbonate precipitation after discharge. Moreover, today's springs are very small, flowing for only a few meters or not at all on the surface. Short residence at the surface appears to result from some combination of re-infiltration into the ground, dewatering by plants growing in the water, and evaporation.

Only the last is a fractionating process for oxygen, and the small difference between vertical and horizontal travertine isotope values indicates evaporation was minimal.

In general, there are no systematic variations in the persistently high $\delta^{18}O_{trav}$ values of >+2‰ over the past 11.5 Ma at Barrancas Blancas (Fig. 7b). Nor do $\delta^{18}O_{water}$ (VSMOW) values (Table 4) reconstructed from $T(\Delta_{47})$ and $\delta^{18}O_{trav}$ values show a discernible temporal pattern. $\delta D_{inclusw}$ show no pattern whereas $\delta^{18}O_{inclusw}$ are higher in the younger samples (e.g. SPN-25 and SPN-12AX in Table 3). We are reluctant to attach any climate significance to this increase, given the small sample size and possibility that oxygen in inclusions could exchange with carbonate oxygen on long time scales (Cole and Chakraborty, 2001), but this issue should be explored with a larger data set.

Overall, it is significant that reconstructed paleo-$\delta^{18}O_{water}$ values overlap that of highly evaporated modern groundwater found only in the driest sector of the Atacama today (Fig. 6). Our results indicate that this has remained the case for much of the last 11.5 Ma, excluding several gaps in our record.

6.2 Carbon isotopic results

To interpret the $\delta^{13}C_{trav}$ values in the Barrancas Blancas record, it is important to first recall that CO_2 dissolved in non-hydrothermal groundwater has four potential sources in the Atacama Desert: the atmosphere, plants, limestone, and volcano-magmatic sources. Of these, a volcano-magmatic source for this CO_2 at Barrancas Blancas over the past 11.5 Ma is the most likely, based on unusually high mean $\delta^{13}C$ values of vertical and horizontal travertine of +5.1 (n= 67) and +5.8‰ (n=70), respectively (Table 2). At 5°C

the calculated $\delta^{13}C$ value of that CO_2 would be about -3 to -4‰ (Romanek et al., 1992), which is much higher than that expected from plant-dominated CO_2. Plants in the Atacama are mainly of the C_3 type with a lesser contribution of C_4 and CAM plants, the two latter photosynthetic plant types have higher $\delta^{13}C$ values, and found mainly at elevations below Barrancas Blancas (Quade et al., 2007). Carbonates formed in the presence of CO_2 from C_3 plants have $\delta^{13}C$ values <<0‰ in soil profiles beneath such plant cover, and in contact with groundwater recharged through those soil profiles. Such values have been observed in springs, rivers and wells from the moister and more vegetated Andes of northern Chile (Fritz et al. 1981). $\delta^{13}C$ values of dissolved inorganic carbon ($\delta^{13}C_{DIC}$) in groundwater and springs in that region average -9.3±2‰, which should produce $\delta^{13}C_{trav}$ of about -8‰, much lower than average values of $\delta^{13}C_{trav}$ from Barrancas Blancas of +5 to +6‰. In contrast to our study area, this plant source of low $\delta^{13}C_{DIC}$ values of groundwater and springs northern Chile is not overwhelmed by volcanic CO_2 from the many active volcanoes in that region.

A purely atmospheric or limestone source is also unlikely for the unusually high $\delta^{13}C_{trav}$ values obtained at Barrancas Blancas. The $\delta^{13}C$ value for pre-modern Cenozoic atmospheric CO_2 is -6.1‰ (Tipple et al., 2010), which should yield values of +3 to +4‰ in associated carbonate. This is too low for observed $\delta^{13}C_{trav}$ values of >+5‰, although we cannot preclude some atmospheric contribution. Limestone can be eliminated as an influence because the watershed is underlain entirely by igneous and volcanoclastic rocks.

This leaves volcano-magmatic CO_2 as the likeliest source of CO_2 dissolved in Barrancas spring water now and in the past. This is not surprising because the recharge

area in the nearby Andes has several active to semi-active volcanoes, and unlike the Andes of northern Chile, it is barely vegetated. In this sector of the Andes, the period 10-1 Ma is characterized by extrusion of enormous volumes (>10,000 km^3) of mainly silicic ignimbrites, referred to as the Altiplano-Puna Volcanic complex, or APVC (de Silva, 1989; de Silva and Gosnold, 2007). The spatial distribution of $\delta^{13}C_{DIC}$ values from groundwater in the nearby Socompa volcano area point to a magmatic subduction zone contribution with $\delta^{13}C$ values for CO_2 of -9 to -4‰ (Rissman et al., 2015). A nearly identical range of values was obtained for hydrothermal waters with presumed purely magmatic sources in northern Chile (Tassi et al., 2010). The higher values in this range would yield the observed +5 to 6‰ for $\delta^{13}C_{trav}$ values at 5-10°C at Barrancas Blancas.

As with $\delta^{18}O_{trav}$ values, there are no systematic variations in the persistently high $\delta^{13}C_{trav}$ values of >+2‰ over the past 11.5 Ma at Barrancas Blancas (Fig. 7a). This leads us to conclude, as did Rech et al. (2010) for the Calama Basin, that the catchment drained by the Barrancas Blancas springs has remained very sparsely vegetated over much of the past 11.5 Ma, as it is today. This has allowed volcanic CO_2 to dominate dissolved inorganic carbon in groundwater, unlike in the Andes of northern Chile where volcanism is also very active but vegetation cover is much greater. The lack of vegetation is consistent with the formal definition of hyperaridity, which is defined by an Aridity Index (=mean annual rainfall/potential evapotranspiration) of <0.05 (UNEP, 1992), a condition generally too dry for plants.

6.3 Comparison to other Regional Paleoclimate Records

The evidence for aridity in the Atacama reaches well back into the Mesozoic (Hartley et al., 2005; Clarke, 2006). Extensive evaporites can be traced back to the Cretaceous-age Purilactis Group (Mpodozis et al., 2005) and the Paleogene (Arriagada et al., 2006), showing that the region was arid but probably not hyperarid before the Miocene. This fits with the fore-arc position of the ancestral Atacama since the mid-Mesozoic, west of a magmatic arc that interdicted easterly moisture, and at a paleo-latitude similar to today. Evaporites are also present as far back as the late Eocene in the western Andes at this latitude, pointing to a very dry and possibly high Andes at that time (Quade et al., 2015) and continuously since then (Vandervoort et al., 1995).

As we regard the Barrancas Blancas work as in-progress, a detailed comparison of our results to other paleoclimate records in the region is premature. However, we will briefly present the main outlines of the scientific evidence for Atacama aridification as it currently stands, beginning with some isotopic results from the Calama Basin, also from the foot of the Andes, but ~230 km north of Barrancas Blancas (Fig. 1). Our results show a remarkable concordance with isotopic records (Fig. 7) collected there by Rech et al. (2010), studying the isotopic composition of palustrine, lacustrine, and spring carbonates. The oxygen and carbon isotopic records from the two areas are virtually indistinguishable where the two records overlap in time <7 Ma. Together, the Calama Basin and Barrancas Blancas records depict a very dry and nearly plantless landscape along the western face of the Andes between ~22 and 25°S during most of the late Neogene. Results for >11.5 Ma only come from the Calama Basin and are somewhat contradictory. $\delta^{13}C$ values from the Calama basin indicate a shift to plant-less conditions sometime between 21 and 12 Ma (Fig. 7a), whereas $\delta^{18}O$ values point to the onset of hyperaridity sometime between

12 and 7 Ma (Fig. 7b). The oxygen isotope records place the onset of hyperaridity at >11.5 Ma for the Barrancas area, and combined with the 12 and 7 Ma interval indicated in the in the Calama Basin, point to a mid-Miocene onset of hyperaridity between latitudes 21-25°S. Similar time gaps in the two widely separated records, most notably between 0-2, 7 to 10 Ma, and >11.5 Ma, raise the question if they are somehow climate related. Future work should address this possibility with more systematic sampling of the deposits at Barrancas Blancas.

Many but not all studies from elsewhere in the Atacama support the idea that the hyperaridity first developed by no later than the mid-Miocene in the region. Dunai et al. (2005) estimates a minimum age of late Oligocene for the onset of hyperaridity, others the Miocene (Alpers and Brimhall, 1988; Sillitoe and McKee, E.H., 1996; Rech et al. 2006; Jordan et al., 2014; Matmon et al., 2015) to Pliocene or later (Hartley and Chong, 2002; Amundson et al., 2012; Jungers et al., 2013). At nearby Escondida, Oerter et al. (2015) suggest that hyperaridity can be no older than 10-20 Ma, based on the presence of pedogenic carbonate in paleosols from that age range. This can be compared to the presence of nitrate–rich soils–a distinguishing feature of the hyperarid core of the Atacama today–that date as far back as ~13 Ma (Rech et al., 2006), providing a robust minimum estimate for the onset of hyperaridity. This is reinforced by evidence for extreme stability of boulder fields in the central Atacama (Matmon et al., 2015) ≤ 12 Ma. The causes of hyperaridification may be due to blocking of easterly moisture sources caused by a step-wise heightening (Garzione et al., 2008) and/or broadening (Quade et al., 2015) of the central Andes in the Miocene. Closure of the Panamanian sea way and

intensification of the Peru Current may be another explanation, although the timing of closure continues to be debated (e.g. Montes et al., 2015; O'Dea et al., 2016).

However, it has been suggested that hyperaridity, once established in the mid-Miocene, gave way to a period or multiple periods (e.g. Jordan et al, 2014) of less dry conditions during the Pliocene, as evidenced by the expansion of lakes during the Pliocene in the Central Depression (Sáez et al., 2012), Calama (de Wet et al., 2015), and Salar de Atacama Basins (Evenstar et al., 2015) (Fig. 1). This change may be related to a permanent El Niño-like state in the Pacific Ocean that developed during the Pliocene (Molnar and Cane, 2002; Haywood et al., 2007). Many of the Atacama studies rely on the physical occurrence of lake deposits during these intervals, whereas dry periods are interpreted to be represented by evaporites or by non-deposition. These and other studies (such as May, 1999) are correct in pointing out the challenge of distinguishing climatic versus tectonic causes of lake development. However, the presence of lake deposits at about the same time in all three basins strengthens the case for a climatic rather than tectonic cause.

Analyses from the Pliocene in both the Barrancas Blancas and Calama isotope records show no clear shift toward lower values during the Pliocene relative to other periods that might indicate less evaporation or more plants. If both lake and isotope records are correct, then the climate changes that led to lake development were not large enough or long enough to change the essentially very dry and plantless character of the watersheds. It is a central goal of future research on the extensive deposits at Barrancas Blancas to fill in the temporal gaps in the record presented in this paper, and to see if the unchanging character of isotopic values for the late Miocene-Pliocene can be replicated.

6.4 Resemblance to groundwater carbonate deposits at Devils Hole, USA

The presence of vertical veins at Barrancas Blancas is geologically rather unusual and presents a research opportunity, because their equivalents at Devils Hole near Death Valley, USA contain what is arguably one of the most remarkable continental isotopic records (DH-11) yet documented. The Devils Hole record is exceptionally well dated and displays oscillations in the $\delta^{18}O$ value of recharge water (Winograd et al., 1992) and $\delta^{13}C$ value of DIC (Coplen et al., 1994) through at least four glacial cycles. Even older deposits in nearby Furnace Creek record changes in inclusion water over the past two million years (Winograd et al., 1985) related to regional climate change and perhaps uplift of the nearby Sierra Nevada Mountains and Transverse Ranges. High U/Pb ratios of the Barrancas Blancas carbonates foreshadow that some of the Plio-Pleistocene samples could be dated at coarse (<100,000 yr) orbital time scales, potentially yielding well-resolved records of paleoenvironmental change for the pre-Quaternary Neogene.

Acknowledgements

It is a pleasure to acknowledge the support of our entire COSA (Convergent Orogenic Systems Analysis) research group, as well as Exxon-Mobil Corporation, its sponsor. We extend our sincere thanks to Amir Sandler for the XRD analysis. We also acknowledge support from NSF-EAR-1156134 to KWH and PFB23 (to the IEB) to CL. This paper benefited from many discussions and comments from Barbara Carrapa, Peter DeCelles, Linda Godfrey, Jerry Kendall, James Mayer, Ari Matmon, Christa Placzek, Jason Rech,

Joellen Russell. Ike Winograd, Kevin Breen, and two anonymous reviewers provided very helpful reviews of the manuscript. Any use of trade, firm, or product names in this paper is for descriptive purposes only and does not imply endorsement by the U.S. Government.

References

Affek, H.P., Eiler, J.M., 2006. Abundance of mass 47 CO_2 in urban air, car exhaust, and human breath. Geochim. Cosmochim. Acta 70, 1-12.

Alpers, C., Brimhall, G.H., 1988. Middle Miocene climatic change in the Atacama Desert, northern Chile: Evidence from supergene mineralization at La Escondida. Geol. Soc. Am. Bull. 100, 1640-1656.

Alpers, C., Whitmore, D.O., 1990. Hydrogeochemistry and stable isotopes of ground and surface waters from two adjacent closed basins, Atacama Desert, northern Chile. Appl. Geochem. 5, 719-734.

Amundson, R., Kelly, E., 1987. The chemistry and mineralogy of a CO_2-rich travertine depositing spring in the California Coast Range. Geochim. Cosmochim. Acta 51 (11), 283-289.

Amundson, R.W., Deitrich, D., Bellugi, S., Ewing, K., Nishizumi, J., Owen, R., Finkel, A, Heimsath, B., Stewart, B., Caffee, M., 2012. Geomorphic evidence for the late Pliocene onset of hyperaridity in the Atacama Desert. Geol. Soc. Am. Bull. 124, 1048-1070.

Aravena, R., Suzuki, O., 1990. Isotopic evolution of river water in the northern Chile region. Water Resources Res. 26 (12), 2887-2895.

Aravena, R., Suzuki, O., Peña, H., Pollastri, A., Fuenzalida, H., Grilli, A., 1999. Isotopic composition and origin of precipitation in northern Chile. Appl. Geochem. 14, 411-422.

Arriagiada, C., Cobbold, P., Roperch, P., 2006, Salar de Atacama Basin; a record of compressional tectonics in the central Andes since the mid-Cretaceous. Tectonics 25, TC1008, doi:10.1029/2004TC001770.

Avigour, A., Magaritz, M., Issar, A., Dodson, M.H., 1990. Sr isotope study of vein and cave calcite from southern Israel. Chemical Geology 82, 69-81.

Betancourt, J. L., Latorre, C., Rech, J. A., Quade, J., Rylander K. A., 2000, A 22,000-year record of monsoonal precipitation from northern Chile's Atacama Desert. Science 289, 1542-1546.

Brand, W., Assonow, S., Coplen, T., 2010. Correction for the ^{17}O interference in $\delta^{13}C$ measurements when analyzing CO_2 with stable isotope mass spectrometry (IUPAC technical report). Pure Appl. Chem. 82(8), 1719-1733.

Canavan, R. R., Carrapa, B., Clementz, M.T., Quade, J., DeCelles, P.G., Shoenbohm, L. M., 2014. Early Cenozoic uplift of the Puna Plateau, central Andes, based on stable isotope paleoaltimetry of hydrated volcanic glass. Geology 42 (5), 447-450.

Clark, I.D., Fritz, P., 1997. Environmental Isotopes in Hydrogeology. Lewis Publishers, 328p.

Clarke, J.D.A., 2006. Antiquity of aridity in the Chilean Atacama Desert. Geomorphology 73, 101-114.

Cole, D.R., Chakraborty, 2001. Rates and mechanisms of isotopic exchange. Reviews of Mineralogy and Gochemistry 43 (1), 83-223.

Cole, J.M., Nienstadt, J., Spataro, G., Rasbury, E.T., Lanzirotti, A., Celestian, A. J., Nilsson, M., Hanson, G.N., 2003. Phosphor imaging as a tool for in situ mapping of ppm levels of uranium and thorium in rocks and minerals. Chem. Geol. 193, 127-136.

Coplen, T. B., Winograd, I. J., Landwehr, J. M., Riggs, A.C., 1994. A 500,000-year stable carbon isotope record from Devils Hole, Nevada. Science 263, 361-365.

Coplen, T.B., 2007, Calibration of the calcite-water oxygen-isotope geothermometer at Devils Hole, Nevada, a natural laboratory. Geochim. Cosmochim. Acta 71, 3948-3957.

Daëron, M., Blamart, D., Peral, M., Affeck, H.P., 2016. Absolute isotope abundance ratios and the accuracy of Δ_{47} measurements. Chem. Geol. 442, 83-96.

De Filippis, L., Faccenna, C., Bolli, A, Anzalone, E., Brilli, M., Ozkul, M.., Soligo, M., Tucckmei, P., Villa, I.M., 2012. Growth of fissure ridge travertines from geothermal springs of Denizli Basin, western Turkey. Geol. Soc. Am. Bull. 124 (9/10), 1629-1645.

de Silva, S., 1989. Altiplano-Puna volcanic complex of the central Andes. Geology 17(12), 1102–1106.

de Silva, S.L., Gosnold, W.D., 2007. Episodic construction of batholiths: Insights from the spatiotemporal development of an ignimbrite flare-up: J. Volcanol. Geo. Res. 167 (1-4), 320–335.

De Wet, C.B., Godfrey, L., de Wet, A.P., 2015. Sedimentology and stable isotopes from a lacustrine-to-palustrine limestone deposited in an arid setting, climatic and tectonic factors: Mio-Pliocene Opache Formation, Atacam Desert, Chile. Palaeogeogr.

Palaeoclimatol. Palaeoecol. 426, 46-67.

Dennis K. J., Affek H. P., Passey, B.H., Schrag D. P., Eiler J. M., 2011. Defining the absolute reference frame for clumped isotope studies of CO_2: Geochim. Cosmochim. Acta 75, 7117-7131.

Dettinger, M., Quade, J., 2015. Calibrating and testing the volcanic glass paleoaltimeter in South America, in: DeCelles, P.G., Ducea, M., Kapp, P., and Carrapa, B. (Eds.), The Geodynamics of a Cordilleran Orogenic System: The Central Andes of Argentina and northern Chile. Geol. Soc. Am. Mem. 212, 261-276.

Dictionary of Geological Terms, 1962. Dolphin Books, Doubleday & Company, Garden City, New York, 545p.

Dunai, T.J., Gonzalez-Lopez, G.A., Jeuz-Larre, J., 2005. Oligocene-Miocene age of aridity in the Atacama Desert revealed by dating of erosion sensitive landforms. Geology 33, 321-324.

Evanstar, L.A., Hartley, A.J., Archert, S.G., Neilson, J.E., 2015. Climatic and halokinetic controls on alluvial-lacustrine sedimentation during compressional deformation, Andean forearc, northern Chile. Basin Res. 1-24, doi: 10.1111/bre12124.

Fiorella, R.P., Poulsen, C.J., Pillco Zolá, R.S., Jeffery, M.L., Ehlers, T., 2015. Modern and long-term evaporation of central Andes surface waters suggests paleo archives underestimate Neogene elevations. Ear. Planet. Sci. Lett. 432, 59-72.

Fritz, P., Suzuki, O., Silva, C., Salati, E., 1981. Isotope hydrology of groundwater in the Pampa del Tamarugal, Chile. J. Hydrol. 53, 161-184.

Garreaud, R.D., Molina, A., and Farias, M., 2010. Andean uplift, ocean cooling and Atacama hyperaridity: A climate modeling perspective. Ear. Planet. Sci. Lett. 292, 39-50.

Garzione, C.N., Hoke, G.D., Libarkin, J., Withers, S., MacFadden, B., Eiler, J., Ghosh, P., Mulch, A., Rise of the Andes. Science 320, 1304-1307.

Gerstenberger, H., Hasse, G., 1997. A highly effective emitter substance for mass spectrometric Pb isotope ratio determinations. Chem. Geol. 136, 309-312.

Godfrey, L.V., Jordan, T.E., Lowenstein, T.K., Alonso, R.L., 2003. Stable isotope constraints on the transport of water to the Andes between 22° and 26°S during the last glacial cycle. Palaeogeogr. Palaeoclimatol. Palaeoecol. 194, 299-317.

Gooseff, M.N., Lyons, B., McKnight, D.M., Vaughn, A., Fountain, A.G., Dowling, C., 2006. A stable isotopic investigation of a polar desert hydrologic system, McMurdo Dry Valleys, Antarctica. Arct. Antarct. Alp. Res. 38(1), 60-71.

Hartley, A.J., G. Chong. 2002. Late Pliocene age for the Atacama Desert: Implications for the desertification of western South America. Geology 30, 43-46.

Hartley, A.J., Chong, G., Houston, J., Mather, A.E., 2005. 150 million years of climatic stability: evidence from the Atacama Desert, northern Chile. J. Geol. Soc. London 162, 421-424.

Haywood, A.M., Valdes, P.J., Peck, V.L., 2007. A permanent El Niño-like state during the Pliocene. Paleoceanography 22, PA1213, doi:10.1029/2006PA001323.

He, B., Olack, G., Colman, A., 2012. Pressure baseline correction and high-precision CO_2 clumped isotope (Δ_{47}) measurements in bellows and micro-volume modes. Rapid. Commun. Mass Spectrom. 26, 2837-2853.

Hill, C.A., Schluter, C.M., Monger, H.C., 1993. Criteria for the recognition of pedogenic/supergene and nonpedogenic/hypogene deposits and their relationship to the origin of calcite/opal deposits at Yucca Mountain. Special report No. 14, submitted to the Nuclear Waste Project Office, State of Nevada, 39p.

Houston, J. and Hartley, A. J., 2003. The central Andean west –slope rainshadow and its potential contribution to the origin of hyperaridity in the Atacama Desert. Int. J. Climatol. 23, 1453-1464.

Huntington K. W., ten others, 2009. Methods and limitations of 'clumped" CO_2 isotope (Δ_{47}) analysis by gas-source isotope ratio mass spectrometry. J. Mass Spectrom. 44, 1318-1329.

Jordan, T.E., Kirk-Lawlor, N.E., Blanco P, N., Rech, J.A., Cosentino, N.J., 2014. Landscape modification in response to repeated onset of hyperarid paleoclimate states since 14 Ma, Atacama Desert, Chile. Geol. Soc. Am. Bull. 126 (7/8), 1016-1046.

Jungers, M.C., Heimsath, A.M., Amundson, R., Balco, G., Shuster, D., Chong, G., 2013. Active erosion-deposition cycles in the hyperarid Atacama Desert of Northern Chile. Ear. Planet. Sci. Lett. 371-372, 125-133.

Kele, S., twelve others, 2015. Temperature dependence of oxygen- and clumped isotope fractionation in carbonates: A study of travertine and tufas in the 6-95°C temperature range. Geochim. Cosmochim. Acta 168, 172-192.

Kelson, J., Huntington, K.W., Schauer, A.J., Saenger, C., Lechler, A.R., 2017. Toward a universal carbonate clumped isotope calibration: Diverse synthesis and preparatory methods suggest a single temperature relationship. Geochim. Cosmochim. Acta 197, 104-131.

Kim, S.-T., O'Neil, J. R., 1997. Equilibrium and non-equilibrium oxygen isotope effects in synthetic carbonates. Geochim. Cosmochim. Acta 61, 3461-3475.

Kluge, T., Affek, H.P., Dublansky, Y., Spötl, C., 2014. Devils Hole paleotemperature and implications for oxygen isotope equilibrium fractionation. Ear. Planet. Sci. Lett. 400, 251-260.

Kluge, T., John, C.M., Jourdan, A.-L., Davis, S., Crawshaw, J., 2015. Laboratory calibration of the calcium carbonate clumped isotope thermometer in the 25-250°C temperature range. Geochim. Cosmochim. Acta 157, 213-227.

Ludwig, K.R., 1993. *PBDAT: A computer program for processing Pb-U-Th isotope data*, version 1.2. USGS Open-File Report 88-542, 30 pp.

Ludwig, K.R., 2003. User's Manual for Isoplot 3.00: A Geochronological Toolkit for Microsoft Excel: Berkeley Geochronological Center Special Publication No. 4, 70 p.

Magaritz, M., Aravena, R., Peña, H., Suzuki, O., Grilli, A., 1989. Water chemistry and isotope study of streams in northern Chile. J. Hydrol. 108, 323-341.

Marty, R., Dunbar, R., Martin, J.B., Baker, P., 1988, Late Eocene diatomite from the Peruvian coastal desert. Coastal upwelling in the eastern Pacific, and Pacific circulation before the terminal Eocene event. Geology 16 (9), 818-822.

Matmon, A., Quade, J., Placzek, C., Fink, D., ASTER Team, Copeland, A. , Nelson, J., 2015. Seismic boulder fields of the Atacama Desert. Geomorphology, 231, 28-39.

Matsuoka, J., Kano, T., Oba, T, Watanbe, T., Sakai, S., Seto, K., 2001. Seasonal variation of stable isotopic compositions recorded in a laminated tufa, SW Japan. Ear. Planet. Sci. Lett. 192, 31-44.

May, G., Hartley, A.J., Stuart, F.M., Chong, G., 1999. Tectonic signatures in arid continental basins: an example from the Upper Miocene-Pleistocene, Calama Basin, Andean forearc, northern Chile. Palaeogeogr. Palaeoclimatol. Palaeoecol. 151, 55-77.

Molnar, P., Cane, M., 2002. El Niño's tropical climate and teleconnections as a blueprint for pre-Ice Age climates. Paleoceanography 17 (2), 1021, 10.1029/2001PA00663.

Montes, C., Cardona, A., Jaramillo, C., Pardo, A., Silva, J.C., Valencia, V., Ayala, C., Pérez-Angel, Rodriguez-Parra, Ramirez, V., Niño, H., 2015. Middle Miocene closure of the Central American Seaway. Science 348, 226–229.

Mpodozis, C., Marinovic, N., Smoje, I., 1993. Eocene left-lateral strike-slip faulting and clock-wise block rotations in the Cordillera de Domeyko, west of Salar de Atacama, northern Chile Second International Symposium on Andean Geodynamics (ISAG), Oxford , UK, Extended Abstracts, 225-228.

Mpodozis, C., Arriagiada, C., Basso, M, Roperch, P., Cobbold, P., Reich, M., 2005. Late Mesozoic to Paleogene stratigraphy of the Salar de Atacama Basin, Antofagasta, northern Chile: implications for the tectonic evolution of the central Andes. Tectonophysics 399, 125-154.

O'Dea, A. and 34 others, 2016. Formation of the Isthumus of Panama. Science Advances 2(8), e1600883 DOI:10.1126/sciadv.1600883.

Oerter, E., Amundson, R., Heimsath, A., Jugers, M., Ching, G., Renne, P., 2015. Early to middle Miocene climate in the Atacama Desert of northern Chile. Palaeogeogr. Palaeoclimatol. Palaeoecol. 10.1016/j.palaeo.2015.10038.

Ortiz, C., Aravena, R., Briones, E., Suárez, F., Tore, C., Muñoz, J.F., 2014. Sources of

surface water for the Soncor ecosystem, Salar de Atacama basin, northern Chile. Hydrolog. Sci. J. 59 (2), 336-350.

Peña, H., 1989. Measurements of ^{18}O and ^{2}H in snow 'penitentes' (IAEA-Technical Document 502-Isotope Hydrology Investigations in Latin America). International Atomic Energy Agency (IAEA), p. 143-154.

Pigati, J.S., Rech, J.A., Quade, J., Bright, J.A., 2014. Desert wetlands in the geologic record. Ann. Rev. Ear. Sci. 132, 67-81.

Quade, J., Rech, J., Latorre, C., Betancourt, J., Gleason, E., Kalin-Arroyo, M., 2007. Soils at the hyperarid margin: the isotopic composition of soil carbonate from the Atacama Desert. Geochim. Cosmochim. Acta 71, 3772-3795.

Quade, J., Rech, J, Betancourt, J., Latorre, C., Quade, B, Fisher, T. and Rylander, K., 2008, Paleowetlands and regional climate change in the central Atacama Desert, northern Chile. Quaternary Res. 69, 343-360.

Quade, J., Dettinger, M., DeCelles, P., Carrapa, B., Huntington, K., Murray, K., 2015. The Growth of the Central Andes 22-26°S, in: DeCelles, P.G., Ducea, M., Kapp, P., and Carrapa, B. (Eds.), The Geodynamics of a Cordilleran Orogenic System: The Central Andes of Argentina and northern Chile. Geol. Soc. Am. Mem. 212, pp. 277-308.

Randall, D.E., 1998. A new Jurassic-recent apparent polar wander path for South America and a review of central Andean tectonic models. Tectonophysics 299, 49-74.

Rech, J.A., Quade, J., Betancourt, J.L., 2002. Late Quaternary paleohydrology of the central Atacama Desert (lat. 22-24°S), Chile. Geol. Am. Soc. Bull. 114 (2), 334-348.

Rech, J.A., B.S. Currie, G. Michalski, A.M. Cowan, 2006. Neogene climate change and uplift in the Atacama Desert, Chile. Geology 34, 761-764.

Rech, J.A., Currie, B.S., Shullenberger, E.D., Dunagan, S.P., Jordan, T.E., Blanco, N., Tomlinson, A.J., Rowe, H.D., Houston, J., 2010. Evidence for the development of the Andean rain shadow from a Neogene isotopic record in the Atacama Desert, Chile. Ear. Planet. Sci. Lett. 292, 371-382.

Rissman, C., Leybourne, M., Benn, C., Christenson, B., 2015. The origin of solutes within the groundwaters of a high Andean aquifer. Chem. Geol. 396, 164-181.

Romanek, C. S., Grossman, E. T., Morse, J. W., 1992. Carbon isotopic fractionation in synthetic aragonite and calcite: effects of temperature and precipitation rate. Geochim. Cosmochim. Acta 56, 419-430.

Sáez, A., Cabrera, L., Garcés, M., van den Bogaard, P., Jensen, A., Gimeno, D., 2012. Stratigraphic record of changing hyperaridity in the Atacama Desert over the last 10 Ma. Ear. Planet. Sci. Lett. 355-356, 32-38.

Schauer, A.J., Kelson, J., Saenger, C., Huntington, K.W., 2016. Choice of ^{17}O correction affects clumped isotope (Δ_{47}) values of CO_2 measured with mass spectrometry. Rapid Commun. Mass Spectrom. 30, 2607-2616.

Sillitoe, R.H., McKee, E.H., 1996. Age of supergene enrichment in the Chilean porphyry copper province. Econ. Geol. Bull. Soc. 91, 164-179.

Stichler, W. Schotterer, U., Frölich, K., Ginot, P., Kull, C., Gäggeler, B. Pouyard, 2001. Influence of sublimation on stable isotope records recovered from high-altitude glaciers in the tropical Andes. J. Geophys. Res. 106 (D19), 22,613-22620.

Sultan, M., Sturchio, N.C., Gheith, H., Abdel Hady Y., and El Anbeawy, M., 2000. Chemical and isotopic constraints on the origin of Wadi El-Tarfa ground water, eastern desert, Egypt. Ground Water 38 (5), 743-751.

Tassi, F., Aguilera, F., Darrah, T., Vaselli, O., Capaccioni, B., Poreda, R. J., Delgado-Huertas, A., 2010. Fluid geochemistry of hydrothermal systems in the Arica-Parincota, Tarapaca, and Antofagasta regions (northern Chile). J. Volcan. Geotherm. Res. 192, 1-15.

Tipple, B.J., Meyers, S.R., Pagani, M., 2010. Carbon isotope ratio of Cenozoic CO_2: a comparative evaluation of available geochemical proxies. Paleoceanography 25, PA3202, doi 10.1029/2009PA0011851.

Usdowski, E., Hoefs, J., Menschel, G., 1979. Relationship between ^{13}C and ^{18}O fractionation and changes in major element composition in a recent calcite-depositing spring—a model of chemical variations with inorganic $CaCO_3$ precipitation. Ear. Planet. Sci. Lett. 42, 267-276.

UNEP (1992) World Atlas of Desertification.

Uysal, T.,Feng, Y., Zhao, J., Altunel, E., Weatherily, D., Karabacak, V., Cengiz, O., Golding, S.D., Lawrence, M.G., Collerson, K.D., 2007. U-series dating and geochemical tracing of late Quaternary travertine in co-seismic fissures, Ear. Planet. Sci. Lett. 257, 450-462.

Vandervoort, D.S., Jordan, T.E., Zeitler, P.K., and Alonso, R.N., 1995. Chronology of internal drainage development and uplift, southern Puna plateau, Argentine central Andes. Geology 23, 145-148.

Vaniman, D.T., Bish, D.L., Chipera, S., 1988. A preliminary comparison of mineral deposits in faults near Yucca Mountain, Nevada, with possible analogs. Los Alamos National Laboratory, Report LA-11289-MS, 54pp.

Vila, T.G., Chong, C.D., 1972. Prospección preliminar de agregados puzolanicos, Provincia Antofagasta. Instituto de Investigaciones Geológicas, Oficina Regional de Antofagasta, 33p.

Vonhof, H.B., van Brueken, M.R., Postma, O., Rowe, P.J., Atkinson, T.C., Kroon, D., 2006. A continuous-flow crushing device for on-line δ^2H analysis of fluid inclusion water in spelethems. Rapid Comm. Mass Spectrom. 20, 2553-2558.

Vonhof, H.B., Atkinson, T.C., Postma, O., van Brueken, M.R., 2007. Fluid inclusion hydrogen and oxygen isotope analyses using the "Amsterdam Device": a progress report. Geophys. Res. Abstr. 9, 05702.

Wierzbowski, H., 2007. Effects of pre-treatments and organic matter on oxugen and carbon isotope analyses of skeletal and organic calcium carbonate. Int. J. Mass Spectrom. 268, 16-29.

Winograd, I. J., Szabo, B., Coplen, T. B., Riggs, A. C., Kolesar, P. T., 1985. A two-million-year record of deuterium depletion in Great Basin ground waters. Science 227, 519-521.

Winograd, I. J., Coplen, T. B., Landwehr, J. M., Riggs, A. C., Ludwig, K. R., Szabo, B. J., Kolesar, P. T., Revesz, K. M., 1992. Continuous 500,000-year climate record from Devils Hole, Nevada. Science 258, 255-260.

Figure captions

Figure 1. Location of the study area at Barrancas Blancas at the foot of the western slope of the Andes. The springs at Barrancas Blancas are fed by recharge from the western

Andes, including the towering Volcán de Llullaillaco (6739m). The regional inset shows the major basins mentioned in the text and the coastal city of Antofagasta.

Figure 2. Map (see Fig. 1 for regional location) of the main travertine occurrences and informal sampling areas A-D at Barrancas Blancas. Spring water and travertine sample locations also shown. Dashed lines mark fault scarps and lines associated with the Barrancas Blancas Fault system. Dot-dashed lines show the channels of ephemeral washes intersecting the travertine deposits.

Figure 3. Photographs of typical occurrences of travertine at Barrancas Blancas. See Figure 2 for locations. (A) Travertine sample SPN-25 (~8 cm high) from area C, 2.079±0.044 Ma, (B) layered sparry calcite from AD10-121, area D, pen for scale, (C) ~1.5 cm thick, reworked chips of layered sparite, AD10-117, area A (D) fault trace localizing travertine, AD10-120, area D, (E) unsampled vertical fissure travertine fill, area A, outcrop ~ 5m high.

Figure 4. Two measured and sampled sections: a) AD10-117 (area A) and b) AD10-121 (area D). Numbers immediately to the right of the stratigraphic columns refer to sample numbers pre-fixed AD10- and listed in in Table 2. $\delta^{18}O$ and $\delta^{13}C$ (VPDB) of carbonates shown on the right side. See Fig. 2 for locations, and Figure 4b for explanation of symbols.

Fig. 5 Tera-Wasserburg plots of U-Pb isotope results from a sample of the Barrancas-Blancas travertines. Ellipses depict percent errors at 2σ.

Figure 6. $\delta^{18}O$ versus δD (VSMOW) values of water analyzed in this study and others (Local Meteoric Water Line or LMWL ($\delta D = 7.8\delta^{18}O+9.7$)—Aravena et al., 1999; Global Meteoric Water Line or GMWL; snow meltwater—Alpers and Whitmore, 1990; local Andes snow and rain (23-24.5°S) —Alpers and Whitmore, 1990 and Godfrey et al., 2003). Fine dotted line is a regression of the local (24.5°S) Atacama groundwater and spring samples only, shown with associated line equation and correlation coefficient.

Shaded in gray are predicted isotopic values (Kim and O'Neil, 1997) of water forming in isotopic equilibrium with Neogene calcite using paleo-temperatures estimated from clumped isotopes in vertical veins only (Table 4). High δD values of fluid inclusion water, which roughly match that of observed ground and spring waters, require that the associated carbonate formed in isotopic equilibrium with spring water that underwent significant evaporation in the recharge area prior to discharge.

Fig. 7 a) $\delta^{13}C$ (VPDB) and b) $\delta^{18}O$ values of travertine carbonate versus age for samples from Barrancas Blancas and the Calama Basin areas.

Table 1 U-Pb dating results

Table 2 Stable isotopic travertine results

Table 3 Stable isotopic water results

Table 4 Clumped isotope results

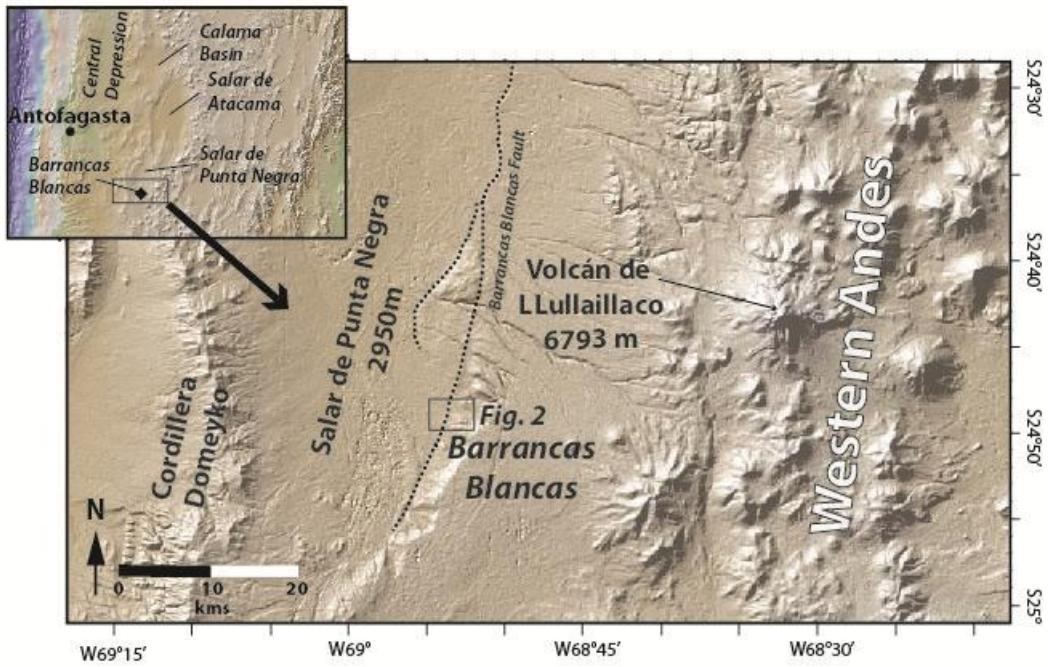

Figure 1 Quade et al.

Figure 1

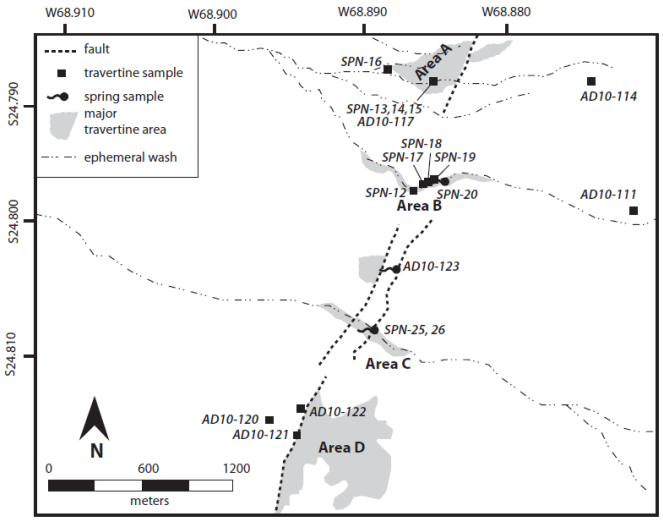

Figure 2 Quade et al.

Figure 2

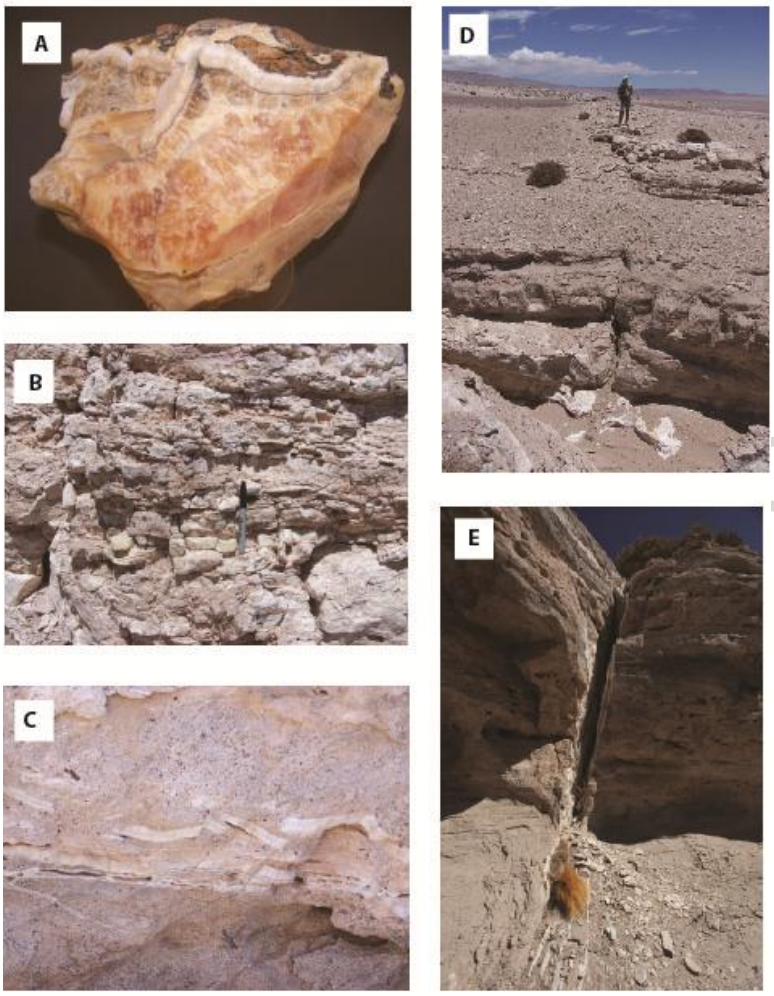

Figure 3 Quade et al.

Figure 3

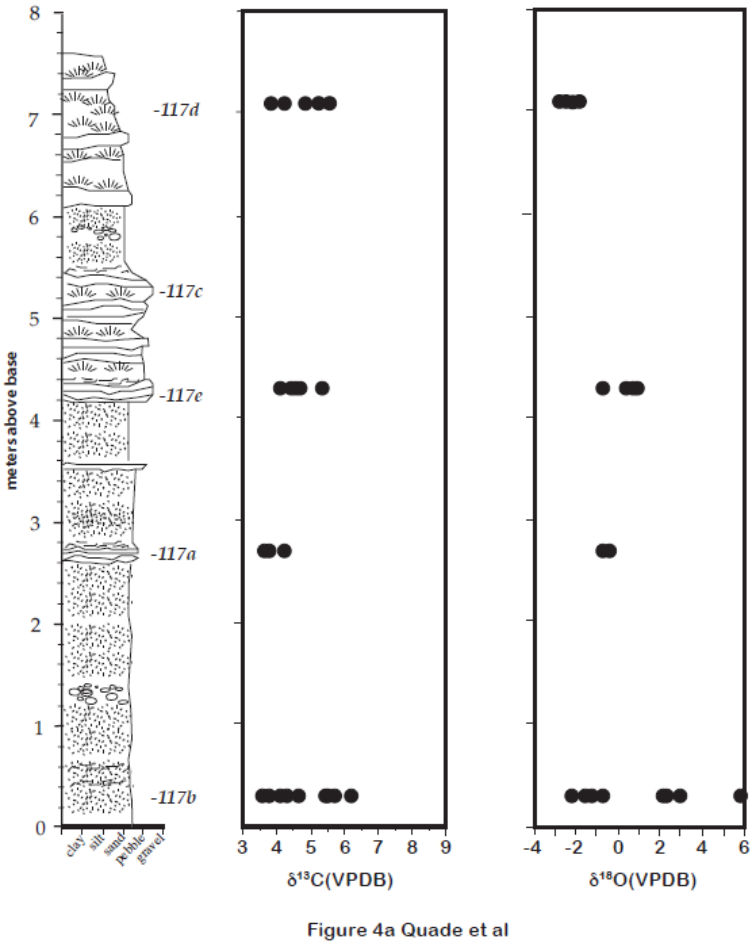

Figure 4a

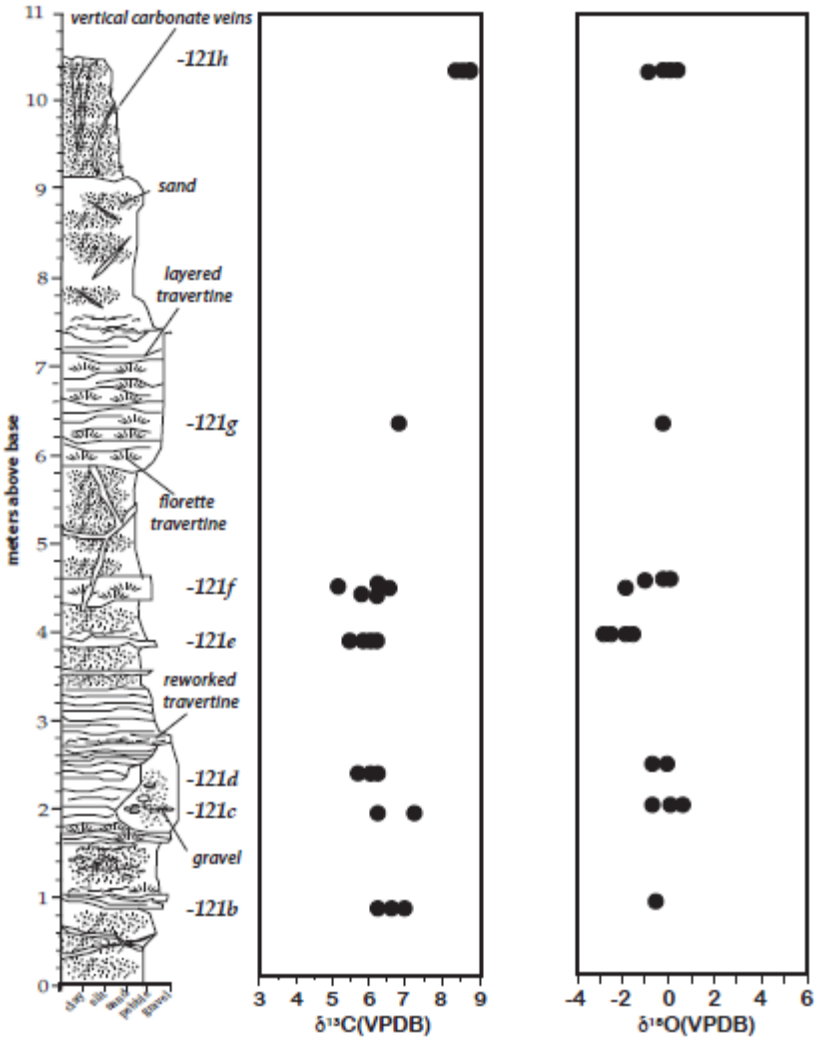

Figure 4b Quade et al

Figure 4b

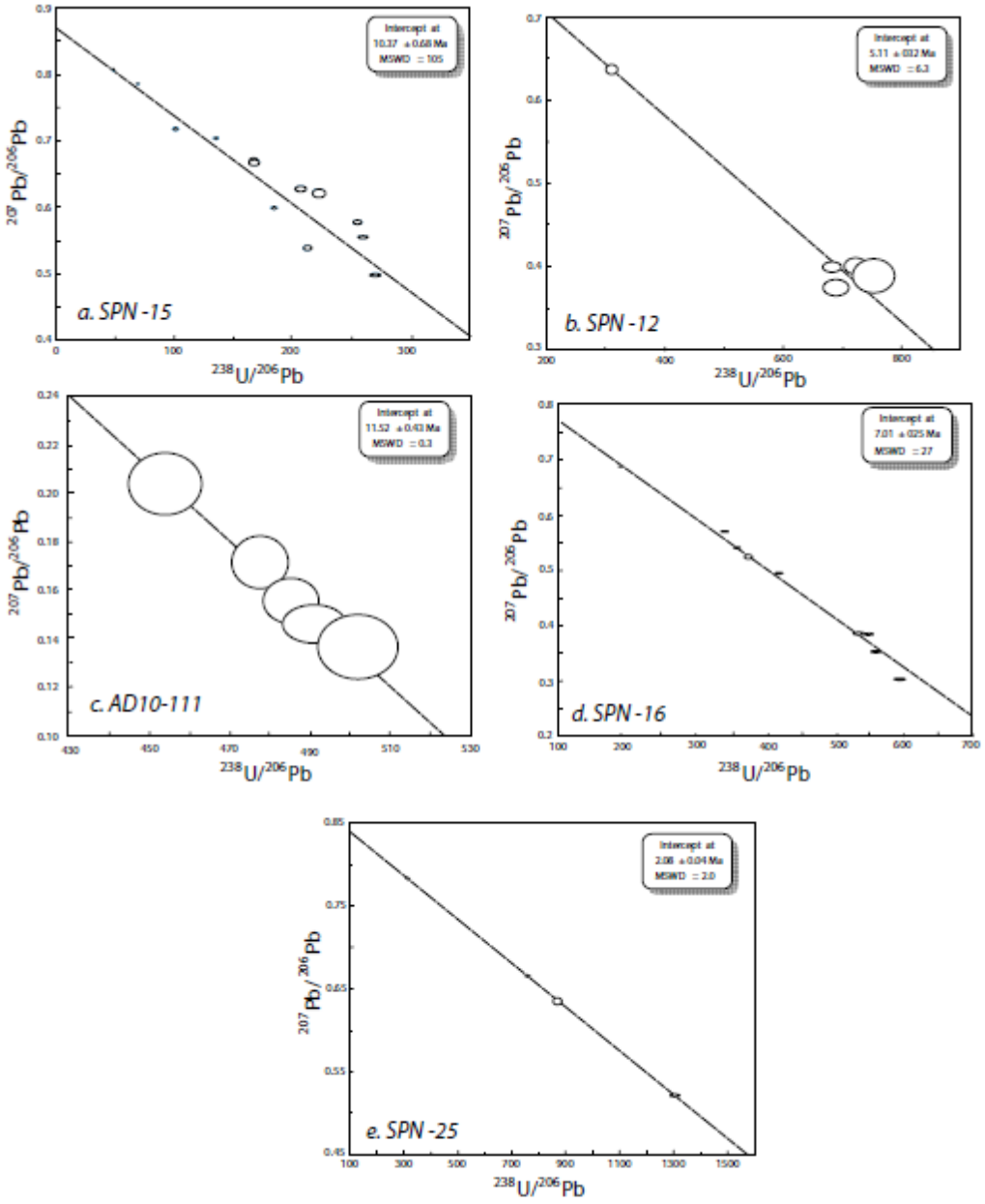

Figure 5 Quade et al.

Figure 5

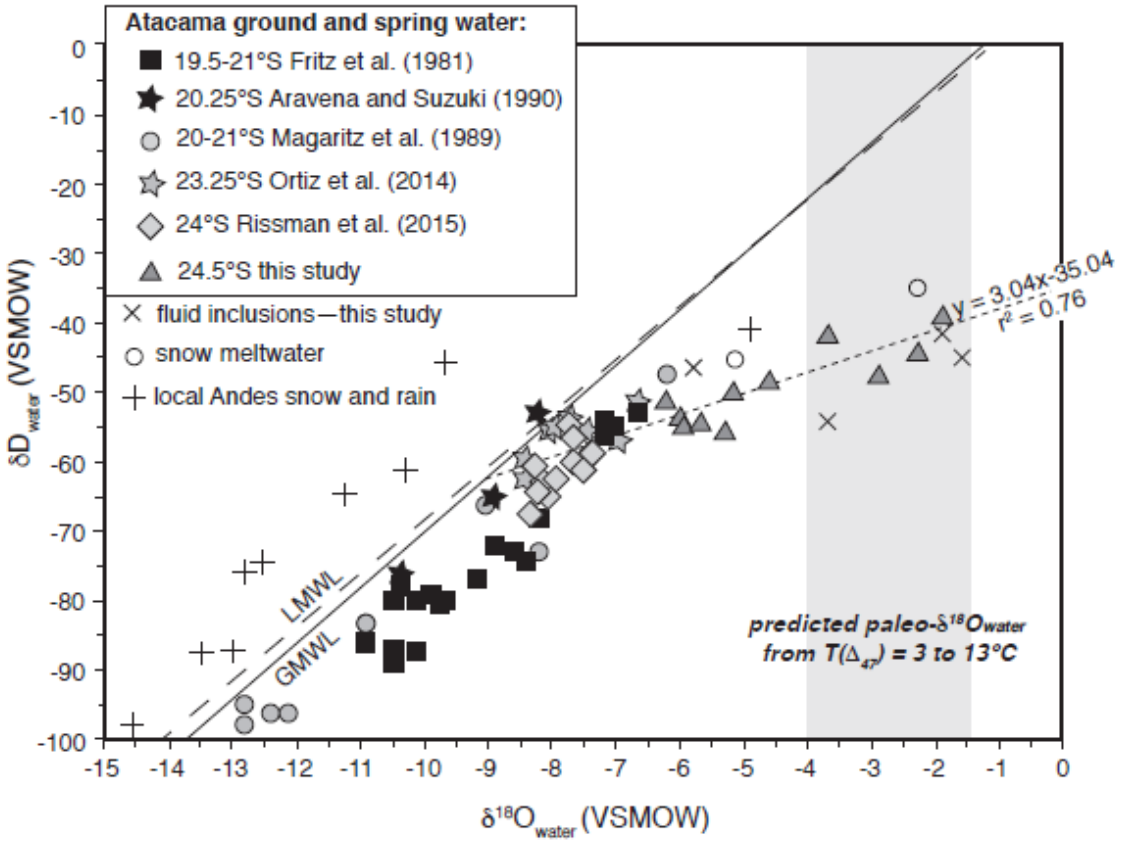

Figure 6 Quade et al.

Figure 6

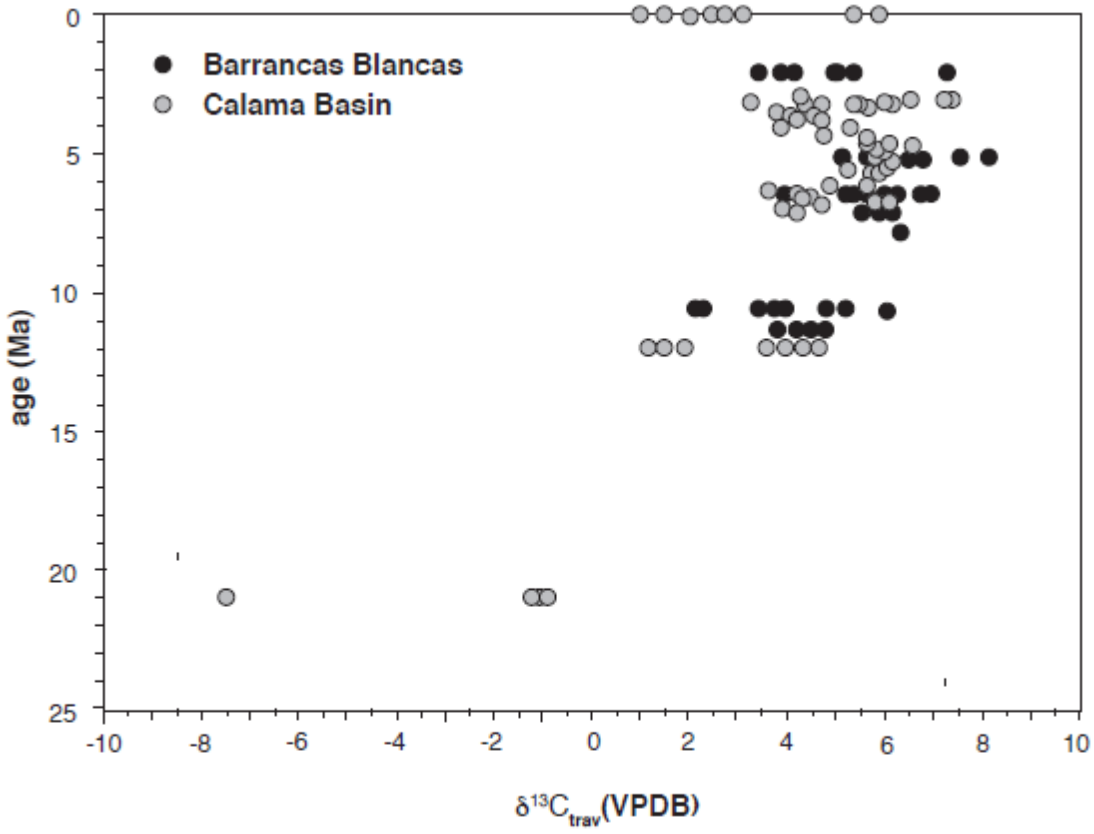

Figure 7a Quade et al.

Figure 7a

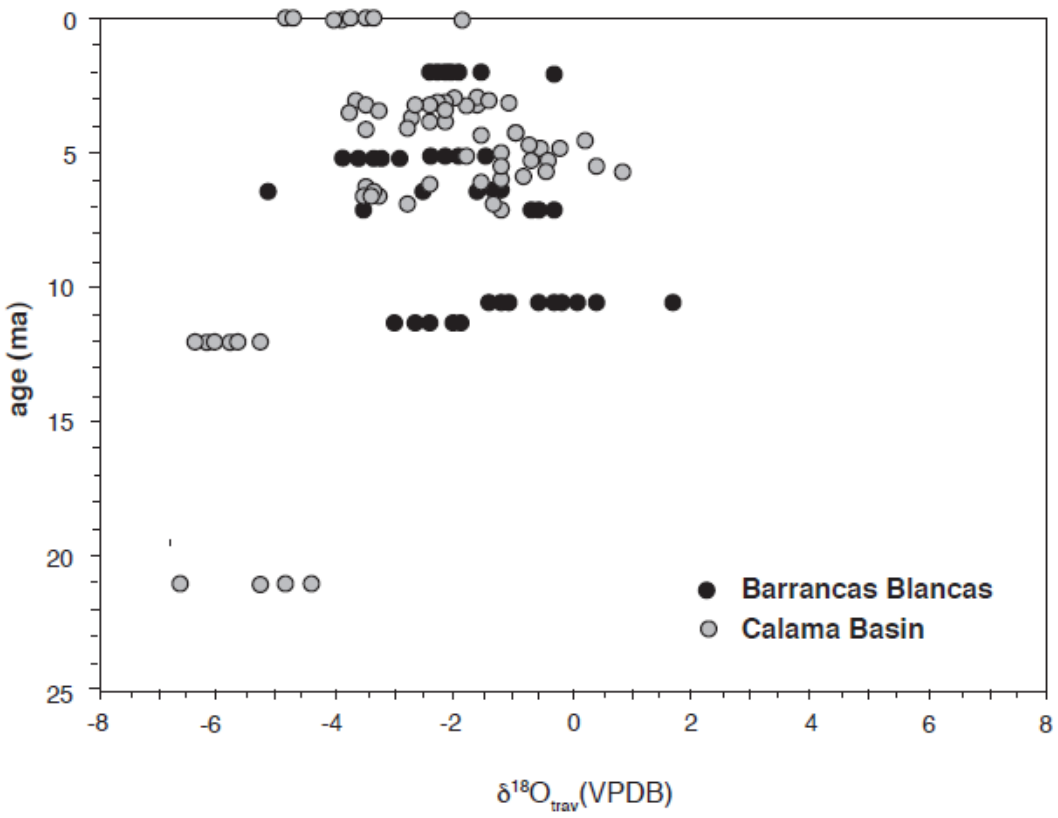

Figure 7b Quade et al.

Figure 7b

TABLE 1 U-Pb AGES

sample	ppm U	±2 (%)	ppm Pb	±2 (%)	$^{238}U/^{204}Pb$	±2 (%)	$^{206}Pb/^{204}Pb$	±2 (%)	$^{207}Pb/^{206}Pb$	±2 (%)
SPN-12										
spn12aYc	17.87	*1.8*	0.05	*1.9*	30578	*4.8*	44.321	*2.4*	0.37475	*2.1*
spn12aYa	19.79	*0.8*	0.06	*1.7*	26911	*4.4*	39.471	*3.5*	0.3996	*1.3*
spn12aWa	9.69	*0.1*	0.09	*2.2*	7713	*3.5*	24.753	*0.8*	0.63863	*0.7*
spn12aYb	17.19	*0.3*	0.05	*2.1*	29687	*4.5*	41.027	*2.2*	0.40001	*2*
spn12ac	11.69	*0.1*	0.03	*3.6*	32170	*9.3*	42.782	*4.7*	0.38903	*4.2*
						age =	***5.11 ± 0.32***		***MSWD=***	***6.3***
SPN-15										
spn15a	3.01	*0.1*	0.03	*1.1*	8102	*2.3*	31.268	*2.3*	0.55498	*0.2*
spn15b	2.86	*0.1*	0.03	*1.1*	6844	*2.3*	26.874	*2.2*	0.57696	*0.4*
spn15c	3.39	*0.2*	0.03	*1.2*	9148	*3.9*	33.912	*3.8*	0.49772	*0.4*
spn15d	2.9	*0.1*	0.03	*1.2*	5779	*4.2*	27.224	*4.1*	0.5381	*0.5*
spn15e	2.89	*0.1*	0.04	*1.1*	5033	*1.6*	27.332	*1.4*	0.59885	*0.2*
spn15f	2.55	*0.1*	0.17	*1*	941	*0.2*	19.424	*0.2*	0.80715	*0.1*
spn15g	2.86	*0.1*	0.13	*1.1*	1381	*0.6*	19.964	*0.4*	0.78569	*0.1*
spn15h	3.02	*0.1*	0.05	*1.6*	4214	*4.1*	25.2	*3.8*	0.66948	*0.4*
spn15i	2.76	*0.2*	0.04	*1.6*	5284	*2.3*	25.563	*0.9*	0.6278	*0.5*
spn15j	3.09	*0.2*	0.07	*1.2*	3053	*1.2*	22.6	*0.5*	0.70366	*0.2*
spn15k	2.9	*0.2*	0.04	*1.7*	5877	*9.7*	26.496	*9.5*	0.62156	*0.7*
spn15l	2.67	*0.1*	0.05	*1.9*	4032	*2.7*	24.049	*0.8*	0.66753	*0.5*
spn15-4	2.64	*0.1*	0.08	*1.7*	2245	*2.3*	22.233	*1.1*	0.71781	*0.3*
						age =	***10.31 ± 0.68***		***MSWD=***	***105***
SPN-16										
spn16a	8.84	*0.1*	0.03	*1.1*	20041	*2.3*	37.402	*2.3*	0.38657	*0.6*
spn16b	8.76	*0.2*	0.03	*1.1*	33180	*3.1*	55.718	*3.1*	0.30347	*0.6*
spn16c	8.53	*0.2*	0.05	*1.1*	12097	*2.1*	32.204	*2*	0.52556	*0.5*
spn16d	7.12	*0.2*	0.02	*1*	26090	*2.1*	46.455	*2*	0.35332	*0.4*
spn16e	8.89	*0.1*	0.03	*1*	23852	*1.6*	43.404	*1.5*	0.38534	*0.3*
spn16f	9.32	*0.1*	0.05	*1*	13639	*0.7*	32.486	*0.6*	0.49577	*0.1*
spn16g	8.97	*0.2*	0.14	*1*	4354	*0.3*	22.92	*0.1*	0.689	*0.1*
spn16h	8.81	*0.1*	0.06	*1*	10687	*0.4*	29.743	*0.3*	0.54216	*0.1*
spn16i	9.38	*0.1*	0.07	*1*	9576	*0.5*	28.038	*0.4*	0.57123	*0.1*
						age	***7.01 ± 0.25***		***MSWD=***	***27***

sample	ppm U	% uncert	ppm Pb	% uncert	$^{238}U/^{204}Pb$	% uncert	$^{206}Pb/^{204}Pb$	% uncert	$^{207}Pb/^{206}Pb$	% uncert
SPN-25										
spn25a	12.89	*0.5*	0.03	*1.4*	21671	*1.5*	24.962	*1*	0.63487	*0.5*
spn25b	13.4	*0.5*	0.14	*1.4*	6309	*1.3*	20.153	*0.8*	0.78377	*0.1*
spn25c	12.59	*0.5*	0.05	*1*	17949	*0.8*	23.666	*0.4*	0.66601	*0.1*
spn25d	13.91	*0.5*	0.03	*1*	40601	*1.4*	31.135	*1.2*	0.52178	*0.2*
spn25e	13.32	*1.8*	0.08	*1.1*	10538	*5.4*	21.37	*5*	0.72435	*0.5*
spn25f	13.42	*0.1*	0.07	*1*	12989	*0.3*	22.124	*0.2*	0.70979	*0.1*
spn25g	12.38	*0.1*	0.06	*1*	13829	*0.3*	22.443	*0.2*	0.70462	*0.1*
spn25h	16.6	*0.2*	0.05	*1*	23515	*0.5*	25.754	*0.2*	0.61553	*0.1*
						age =	***2.079 ± 0.044***		***MSWD=***	***2***
AD10-111										
AD111-1	58.62	*0.1*	0.15	*1.7*	62946	*8.7*	128.184	*7.9*	0.14627	*4.5*
AD111-2	49.01	*0.1*	0.13	*1.5*	63283	*7.9*	130.329	*6.7*	0.15514	*4.9*
AD111-3	45.81	*0.1*	0.13	*1.5*	53359	*7.1*	111.712	*5.9*	0.17169	*4.5*
AD111-4	36.42	*0.1*	0.09	*1.8*	72518	*12.7*	144.404	*11.1*	0.13704	*7.9*
AD111-5	31.34	*0.1*	0.1	*1.9*	40706	*8.1*	89.613	*6.2*	0.20405	*5.1*
						age =	***11.52 ± 0.43***		***MSWD=***	***0.3***

TABLE 2 STABLE CARBON AND OXYGEN ISOTOPE RESULTS FROM TRAVERTINES AND HYDROGEN RESULTS FROM BARRANCAS BLANCAS

Carbonate

SAMPLE ID	age (Ma)	δ^{13}C VPDB (‰)	δ^{18}O VPDB (‰)	remarks
SPN-12				
SPN-12AX-1	NA	6.34	-3.51	vertical vein
SPN-12AX-2	NA	6.85	-3.92	vertical vein
SPN-12AX-3	NA	6.20	-1.44	vertical vein
SPN-12AX-4	NA	4.63	-0.38	vertical vein
SPN-12AX-5	NA	5.36	-2.80	vertical vein
SPN-12AX-6	NA	8.82	-3.61	vertical vein
SPN-12AY-1	NA	6.98	-3.54	vertical vein
SPN-12AY-2	NA	6.91	-3.29	vertical vein
SPN-12AZ-2	NA	7.61	-3.34	vertical vein
SPN-12AZ-3	NA	6.67	-3.82	vertical vein
SPN 12B-X-1	5.11±0.32	5.18	-1.78	vertical vein
SPN 12B-X-2	5.11±0.32	6.51	-1.91	vertical vein
SPN 12B-X-3	5.11±0.32	5.69	-0.60	vertical vein
SPN 12B-X-4	5.11±0.32	5.60	-2.15	vertical vein
SPN 12B-X-5	5.11±0.32	5.12	-3.57	vertical vein
SPN 12B-X-6	5.11±0.32	6.77	-2.18	vertical vein
SPN-12B-X-7	5.11±0.32	8.22	-2.35	vertical vein
SPN 12B-X-8	5.11±0.32	6.12	-1.40	vertical vein
SPN 12B-U-1	5.11±0.32	8.16	-2.95	vertical vein
SPN-12B-U-2	5.11±0.32	7.54	-3.18	vertical vein
SPN-12B-U-3	5.11±0.32	6.62	-1.46	vertical vein
SPN-13				
SPN 13A-1	NA	5.19	-1.14	vertical vein
SPN-13A-2	NA	5.69	-1.76	vertical vein
SPN-13A-3	NA	5.79	-1.09	vertical vein
SPN-13A-4	NA	5.54	-0.51	vertical vein
SPN-13D-1	NA	4.78	-1.47	vertical vein
SPN-13D-2	NA	5.08	-1.43	vertical vein
SPN-13D-3	NA	5.30	-2.04	vertical vein
SPN-13D-4	NA	5.51	-1.91	vertical vein
SPN-13D-5	NA	5.43	-1.59	vertical vein
SPN-13D-6	NA	5.36	-1.02	vertical vein

SPN-14				
SPN-14A-BX-1	6.4±0.61	6.27	-1.56	vertical vein
SPN-14A-BX-2	6.4±0.61	6.00	-1.31	vertical vein
SPN-14A-BX-3	6.4±0.61	5.39	-1.19	vertical vein
SPN-14A-BX-4	6.4±0.61	3.95	-5.10	vertical vein
SPN-14A-BX-5	6.4±0.61	5.19	-1.49	vertical vein
SPN-15				
SPN-15A-1	10.31±0.68	3.90	-1.02	horizontal
SPN-15A-2	10.31±0.68	4.04	-1.35	horizontal
SPN-15A-3	10.31±0.68	4.04	-0.49	horizontal
SPN-15A-4	10.31±0.68	6.05	-0.18	horizontal
SPN-15A-5	10.31±0.68	5.15	-0.20	horizontal
SPN-15B-1	10.31±0.68	5.26	1.66	horizontal
SPN-15B-2	10.31±0.68	4.87	-0.08	horizontal
SPN-15B-3	10.31±0.68	3.41	0.44	horizontal
SPN-15B-4	10.31±0.68	2.09	-0.32	horizontal
SPN-15B-5	10.31±0.68	2.22	-1.13	horizontal
SPN-15C-1	10.31±0.68	3.52	0.16	horizontal
SPN-15C-2	10.31±0.68	3.88	0.20	horizontal
SPN-15C-3	10.31±0.68	4.82	0.35	horizontal
SPN-15C-4	10.31±0.68	3.77	0.22	horizontal
SPN-16				
SPN-16-1	NA	0.94	5.04	horizontal down slope
SPN-16-2	7.01±0.25	5.61	-0.68	horizontal down slope
SPN-16-3	7.01±0.25	5.90	-0.39	horizontal down slope
SPN-16-4	7.01±0.25	5.99	-0.28	horizontal down slope
SPN-16-5	7.01±0.25	6.17	-0.53	horizontal down slope
SPN-16-6	7.01±0.25	5.74	-3.53	horizontal down slope
SPN-17				
SPN-17D-1	NA	5.90	1.10	vertical vein
SPN-17D-2	NA	6.36	-1.34	vertical vein
SPN-17D-3	NA	7.13	-1.33	vertical vein
SPN-17D-4	NA	6.33	-2.09	vertical vein
SPN-18				
SPN-18A-DA-1	NA	6.94	-2.48	vertical vein
SPN-18A-DA-2	NA	6.75	-1.56	vertical vein

SPN-18A-DA-3	NA	5.68	-1.55	vertical vein
SPN-19				
SPN-19B-2	NA	5.92	-3.45	vertical vein
SPN-19B-2	NA	5.77	-1.84	vertical vein
SPN-19B-4	NA	6.80	-2.51	vertical vein
SPN-19B-5	NA	6.52	-1.42	vertical vein
SPN-19B-6	NA	6.33	-2.28	vertical vein
SPN-19B-7	NA	5.97	-0.61	vertical vein
SPN-19B-1	NA	5.66	-0.73	vertical vein
SPN-25				
SPN-25-1	2.079±0.044	4.12	-0.34	vertical vein
SPN-25-2	2.079±0.044	4.99	-2.26	vertical vein
SPN-25-3	2.079±0.044	5.40	-1.89	vertical vein
SPN-25-4	2.079±0.044	7.26	-1.52	vertical vein
SPN-25-5	2.079±0.044	5.00	-1.91	vertical vein
SPN-25-6	2.079±0.044	5.11	-2.11	vertical vein
SPN-25-7	2.079±0.044	3.41	-2.39	vertical vein
SPN-25-8	2.079±0.044	3.88	-1.53	vertical vein
AD10-107				
AD10-107(1)	NA	3.80	-0.90	horizontal below rip up
AD10-107(2)	NA	3.70	-1.21	horizontal below rip up
AD10-107(3)	NA	3.66	-1.39	horizontal below rip up
AD10-107(4)	NA	4.48	-0.28	horizontal below rip up
AD10-111				
AD10-111(1)	11.52±0.43	4.57	-2.06	horizontal
AD10-111(2)	11.52±0.43	4.46	-1.83	horizontal
AD10-111(3)	11.52±0.43	4.24	-2.40	horizontal
AD10-111(4)	11.52±0.43	3.86	-2.62	horizontal
AD10-111(5)	11.52±0.43	4.76	-3.03	horizontal
AD10-114a				
AD10-114a(1)	NA	4.23	-1.43	horizontal
AD10-114a(2)	NA	3.74	-1.99	horizontal
AD10-114a(3)	NA	9.39	1.21	horizontal
AD10-114a(4)	NA	4.88	-0.88	horizontal
AD10-117				

AD10-117B1(1)	NA	3.59	-2.20	reworked travertine
AD10-117B2(1)	NA	3.73	-2.00	reworked travertine
AD10-117B2(3)	NA	3.96	-1.95	reworked travertine
AD10-117B3(2)	NA	3.96	-2.04	reworked travertine
AD10-117B4(2)	NA	4.48	-1.46	reworked travertine
AD10-117B5(1)	NA	5.42	5.75	reworked travertine
AD10-117B5(2)	NA	5.53	3.00	reworked travertine
AD10-117B6(1)	NA	4.59	-1.71	reworked travertine
AD10-117B6(2)	NA	4.68	-1.69	reworked travertine
AD10-117B6(3)	NA	4.00	-1.32	reworked travertine
AD10-117B7(1)	NA	4.35	-1.50	reworked travertine
AD10-117B7(2)	NA	3.81	-1.60	reworked travertine
AD10-117B8(1)	NA	4.14	2.29	reworked travertine
AD10-117B8(2)	NA	4.03	2.10	reworked travertine
AD10-117B9(1)	NA	5.74	-0.70	reworked travertine
AD10-117B9(2)	NA	6.20	-0.75	reworked travertine
AD10-117B1(2)	NA	4.53	-1.37	reworked travertine
AD10-117B2(2)	NA	4.34	-1.52	reworked travertine
AD10-117B3(1)	NA	4.02	-1.91	reworked travertine
AD10-117B4(1)	NA	3.47	-2.17	reworked travertine
AD10-117D(1)	NA	3.84	-2.62	horizontal travertine
AD10-117D(2)	NA	4.84	-2.12	horizontal travertine
AD10-117D(3)	NA	4.25	-2.76	horizontal travertine
AD10-117D(4)	NA	5.59	-1.95	horizontal travertine
AD10-117D(5)	NA	5.16	-2.06	horizontal travertine
AD10-117A(1)	NA	3.80	-0.71	horizontal travertine below rip up
AD10-117A(2)	NA	3.66	-0.53	horizontal travertine below rip up
AD10-117A(3)	NA	4.21	-0.47	horizontal travertine below rip up
AD10-117E(1)	NA	4.67	-0.83	horizontal travertine below rip up
AD10-117E(2)	NA	5.34	0.53	horizontal travertine below rip up
AD10-117E(3)	NA	4.56	0.88	horizontal travertine below rip up
AD10-117E(4)	NA	4.41	0.64	horizontal travertine below rip up
AD10-117E(5)	NA	4.12	0.35	horizontal travertine below rip up
AD10-120				
AD10-120(1)	NA	7.91	-0.21	inclined
AD10-120(2)	NA	8.21	-0.02	inclined

AD10-120(3)	NA	8.07	0.75	inclined
AD10-120(4)	NA	7.60	0.12	inclined
AD10-121				
AD10-121A(1)	NA	6.04	-0.98	vertical vein
AD10-121A(2)	NA	6.83	-1.11	vertical vein
AD10-121A(3)	NA	5.80	-1.18	vertical vein
AD10-121B(1)	NA	6.62	-1.01	horizontal below rip up
AD10-121B(2)	NA	6.36	-1.01	horizontal below rip up
AD10-121B(3)	NA	5.97	-1.10	horizontal below rip up
AD10-121C(1)	NA	6.03	-0.04	horizontal below rip up
AD10-121c(2)	NA	6.86	-0.39	horizontal below rip up
AD10-121c(3)	NA	6.88	-1.46	horizontal below rip up
AD10-121d(1)	NA	5.81	-1.38	horizontal below rip up
AD10-121d(2)	NA	5.47	-0.72	horizontal below rip up
AD10-121d(3)	NA	5.95	-1.30	horizontal below rip up
AD10-121e(1)	NA	5.65	-2.40	horizontal below rip up
AD10-121e(2)	NA	5.97	-3.39	horizontal below rip up
AD10-121e(3)	NA	5.35	-3.18	horizontal below rip up
AD10-121e(4)	NA	6.01	-2.60	horizontal below rip up
AD10-121e(5)	NA	5.86	-2.71	horizontal below rip up
AD10-121f(1)	NA	4.98	-1.58	horizontal
AD10-121f(2)	NA	6.25	-0.84	horizontal
AD10-121f(3)	NA	5.96	-0.47	horizontal
AD10-121g(1)	NA	6.65	-0.89	horizontal
AD10-121g(2)	NA	5.57	-2.49	horizontal
AD10-121g(3)	NA	5.94	-2.58	horizontal
AD10-121h(1)	NA	8.26	-0.17	horizontal
AD10-121h(2)	NA	8.10	-0.79	horizontal
AD10-121h(3)	NA	7.93	-1.44	horizontal
AD10-121h(4)	NA	7.89	-0.63	horizontal
AD10-122				
AD10-122(1)	NA	2.52	-3.62	vertical vein
AD10-122(2)	NA	2.77	-3.32	vertical vein
AD10-122(3)	NA	2.78	-3.40	vertical vein
AD10-122(4)	NA	3.62	-0.87	vertical vein
AD10-122(5)	NA	6.48	-0.60	vertical vein
AD10-122(6)	NA	6.27	0.08	vertical vein

TABLE 3 STABLE HYDROGEN AND OXYGEN ISOTOPE RESULTS FROM SPRINGS, WELLS, AND FLUID INCLUSIONS

Spring and well water

Barrancas Blancas	sample year	$\delta^{18}O$ VSMOW (‰)	δD VSMOW (‰)	
SPN-20A	2004	-5.9	-54.4	north spring
SPN-20A	2010	-1.9	-39	
SPN-20B	2004	-4.6	-48.0	north spring
SPN 26	2004	-2.3	-43.9	south spring
SPN 26	2010	-2.9	-47	
AD10-123	2010	-5.3	-55	small seep
Agua Caliente #3		-5.7	-54.0	Salar de Agua Caliente spring
Imilac spring		-6.2	-50.8	Imilac bathtub
SPN-28		-3.7	-41.5	salar well near station

Fluid Inclusions

SPN-12 Ax		0.67	-46.7	
SPN-12 Ax		-3.24	-45.6	
SPN-12 Ax		-3.10	-31.3	
average		**-1.89**	**-41.19**	
SPN-15		-7.45	-57.6	
SPN-15		-4.09	-35.2	
average		**-5.77**	**-46.41**	
SPN-16		-4.79	-57.5	
SPN-16		-2.53	-49.9	
average		**-3.66**	**-53.69**	
SPN-25		-2.12	-57.3	
SPN-25		-1.07	-32.4	
average		**-1.60**	**-44.83**	

Table 4 Clumped isotope results

Sample ID	Mass (mg)	$\delta^{13}C$ (VPDB)	± 1 SE	$\delta^{18}O$ (VPDB)	± 1 SE	(90° C acid) Δ_{47}	± 1 SE	based on long-term standards ± 1SE	Kelson et al. T(D4	analytical ±	Kim and O'Neil α^-	calculated $\delta^{18}O_{wat}$

									7) (°C)^	1SE		er (SMOW)
AD10-111	6.576	4.242	0.004	-2.811	0.007	0.661	0.009					
	6.663	4.235	0.004	-2.802	0.006	0.613	0.008					
	7.079	4.028	0.005	-2.761	0.008	0.649	0.007					
	7.280	3.945	0.004	-2.741	0.006	0.636	0.008					
	average (1SE):	***4.117***	***0.007***	***-2.782***	***0.002***	***0.640***	***0.010***	0.014	***13***	***4***	1.0311	-3.0
SPN12-AY-1,2	6.961	6.953	0.005	-2.516	0.006	0.666	0.008					
	7.318	6.952	0.005	-2.548	0.006	0.656	0.008					
	7.054	6.904	0.004	-2.524	0.006	0.659	0.008					
	8.316	6.925	0.004	-2.443	0.008	0.652	0.008					
	average (1SE):	***6.931***	***0.010***	***-2.512***	***0.002***	***0.658***	***0.000***	0.014	***8***	***4***	1.0323	-3.8

						3						
			0.		0.		0.					
SPN1			0	-	0		0					
2-AZ-		6.65	0	2.73	0	0.66	0					
1	7.480	5	4	6	7	9	9					
			0.		0.		0.					
			0	-	0		0					
		6.64	0	2.77	0	0.67	0					
	6.924	9	4	6	7	4	7					
			0.		0.		0.					
			0	-	0		0					
		6.67	0	2.70	0	0.61	0					
	7.306	7	5	5	6	9	8					
			0.		0.		0.					
			0	-	0		0					
		6.60	0	2.67	0	0.67	0					
	7.070	6	4	7	6	2	9					
							0.					
	avera		***0.***		***0.***		***0***					
	ge		***0***	***-***	***0***	***0.65***	***1***				1.032	
	(1SE):	***6.65***	***1***	***2.72***	***2***	***9***	***3***	0.014	***8***	***4***	3	-4.0
SPN-			0.		0.		0.					
14-			0	-	0		0					
BX-		6.29	0	1.53	0	0.68	1					
1,2	7.901	8	5	7	7	0	0					
			0.		0.		0.					
			0	-	0		0					
		6.37	0	1.50	0	0.66	0					
	8.561	8	4	3	7	4	9					
			0.		0.		0.					
			0	-	0		0					
		6.33	0	1.49	0	0.69	0					
	6.702	6	5	5	6	2	8					
							0.					
	avera		***0.***		***0.***		***0***					
	ge		***0***	***-***	***0***	***0.67***	***0***				1.033	
	(1SE):	***6.34***	***9***	***1.51***	***1***	***9***	***8***	0.016	***3***	***4***	5	-4.0
			0.		0.		0.					
SPN-			0		0		0					
15B-		4.50	0	0.35	0	0.64	0					
1,2	6.981	9	4	5	7	7	9					
			0.		0.		0.					
		4.52	0	0.40	0	0.66	0					
	7.226	9	0	5	0	1	0					

		5		7		9					
		0.		0.		0.					
		0		0		0					
	4.55	0	0.42	0	0.67	1					
7.002	2	5	6	7	4	0					
		0.		0.		0.					
		0		0		0					
	4.51	0	0.44	0	0.68	0					
7.623	3	5	4	7	4	7					
						0.					
avera		***0.***		***0.***		***0***					
ge		***0***		***0***	***0.66***	***0***			1.032		
(1SE):	***4.53***	***1***	***0.41***	***2***	***7***	***8***	0.014	***6***	***4***	8	-1.4

Long-term standard deviation (SD) in D47 for internal lab standards: SD C2: 0.028 per mil (n=33); SD C64: 0.030 per mil (n=109), SD Cor: 0.031 (n=54);

SD ETH1: 0.013 per mil (n=4); SD ETH2: 0.015 per mil (n=8); SD ETH4: 0.012 per mil (n=4)

Sample standard error (SE) is calculated as $0.028/n^{0.5}$, where n is the number of externally replicated sample analyses, or as the SE of replicate analyses, whichever is larger.

^ using Δ_{47} =(41700/T^2)+0.13, modified equation 1 from Kelson et all. (2017), where T is in Kelvin, with no D47 acid correction; calibration data calculated using Brand et al. (2010) parameters

α^- using $1000\ln\alpha_{calcite\text{-}water}$ =(18030/T-32.42) from Kim and O'Neil (1997), where T is in Kelvin.